MASTER THESIS

VASCULAR PATTERN OF THE FINGER: BIOMETRIC OF THE FUTURE ?

SENSOR DESIGN, DATA COLLECTION AND PERFORMANCE VERIFICATION

B. Ton

FACULTY OF ELECTRICAL ENGINEERING, MATHEMATICS AND COMPUTER SCIENCE.
SIGNALS AND SYSTEMS

EXAMINATION COMMITTEE
dr. ir. R.N.J. Veldhuis
dr. ir. F. van der Heijden
prof. dr. ir. C. H. Slump
prof. dr. J.C.T. Eijkel

DOCUMENT NUMBER
EEMCS – 2012-011

UNIVERSITY OF TWENTE.

3RD JULY 2012

Summary

The usage of the vascular pattern of the finger is emerging as a new form of biometrics. This new biometrics is already commercially exploited but the scientific research done is still lacking behind. The goal of this research is to bridge this gap between research and commerce. In order to do so this research focuses on three main aspects. The first aspect is the design of a sensor capable of capturing the vascular pattern of the finger. At present there are only a small number of datasets publicly available. This is why the second focus point is the collection of a dataset which will be publicly available for further research. The last aspect focuses on the verification of five existing state of the art algorithms.

The dataset collected comprises 59 volunteers which had their ring, middle and index fingers captured from both hands during two sessions. These sessions were separated by two weeks and during each session each finger was captured twice. The collected dataset is noteworthy as the collected images are of high quality and meta-information about the volunteers has been recorded.

The verification experiments have been done using an existing dataset and the collected dataset. For all cases the collected dataset performed better than the existing dataset. Equal Error Rates(EER) down to 0.37% have been achieved for the collected dataset.

Contents

Chapter 1

Introduction

The vascular pattern of the finger is advertised as a promising new biometric, characterized by very low error rates, good spoofing resistance and a user convenience that is equivalent to that of fingerprint recognition. This new form of biometrics has been gaining increasing attention since the year 2000. At present Hitachi has a monopoly position on this new type of biometrics. As a result there are only few and small publicly available datasets and only little academic research has been done in order to verify published claims on performance. Also the various aspects of designing a suitable sensor for capturing vascular pattern images is never extensively elaborated on.

Despite the fact that little academic research has been done on this new biometric, this new biometric is already in use for devices such as automatic teller machines(ATM) and vending machines. These machines are mainly situated in Japan. Also close to home this new form of biometrics has emerged, in 2010 the first ATM with this new form of biometrics was taken into use by the Polish BPS bank [29].

The goal of this research is to get a better understanding of this new form of biometrics and bridge the gap between commerce and academic research. The three major topics covered in this research are the design of the sensor which is capable of capturing a vascular pattern image of the finger, collecting a dataset and the performance verification of several existing algorithms. At the end of this thesis the question whether vascular pattern biometrics has the potential to become the biometric of the future can be answered.

This thesis is composed of six themed chapters. To get familiar with the subject of vascular pattern biometrics a literature research is done first in Chapter 2. Before a dataset can be collected a sensor has to be designed first. The various aspects of designing such a sensor are given in Chapter 3. After the sensor has been designed and constructed a dataset can be collected. Details about the data collection is given in Chapter 4. With the collected dataset various algorithms mentioned in the literature can be tested. The details about these algorithms are given in Chapter 5 and the performance results of these algorithms have been recorded in Chapter 6. At the end of this thesis several conclusions and recommendations for future work will be given.

As a final note it should be mentioned that in this thesis the term *vascular pattern* is used instead of the more popular *vein*. This done because the term vein might induce that only the veins are captured by the sensor device, this is of coarse not true. Both veins and arteries are captured, hence the name vascular pattern is preferred.

Chapter 2

Literature study

This chapter will provide an overview of the available literature regarding the design of an imaging device to capture the vascular pattern of the finger. Also the literature regarding the feature extraction is investigated. This chapter is divided into four main parts, the first part is about the finger itself and will discuss what properties of the finger are relevant for capturing a good vascular image of the finger. The second part is about the imaging device, especially the type of light source is extensively treated, the type of camera and the available commercial devices are discussed briefly. The third part deals with the algorithms which are used for feature extraction and it will also provide a list of performance figures of several different algorithms. At the end of this chapter a few remarks about existing finger vascular pattern datasets are made.

2.1 The finger

The finger is of vital importance when designing a finger vascular pattern imaging device. The first subsection will discuss the properties of the finger which can influence the image quality. The second subsection will mention some anthropometric measurements of the finger such as the average finger length and average finger breadth. These anthropometric measurements are important when designing an imaging device.

All the investigated literature capture the vascular pattern of the ventral side of the finger. The ventral side of the finger is the side which has a fingerprint. The thumb is never imaged in existing literature because it is probably to short and too stubby. To get an impression of how the vascular pattern of the finger will look like an angiogram of the hand is given in Figure 2.1. An angiogram is obtained by injecting a contrast fluid into the blood vessel and capturing the image using some kind of X-ray based technique. From this figure it can be seen that the vascular pattern in the fingertip is very dense. This is probably the reason that in the existing literature the vascular pattern of the fingertip is never clearly visible.

In order to make clear statements about the finger position and rotations an object coordinate system is defined. The definition in this research is equivalent to the one used by the ISO/IEC 19794-9:2011 standard which is given in Figure 2.2.

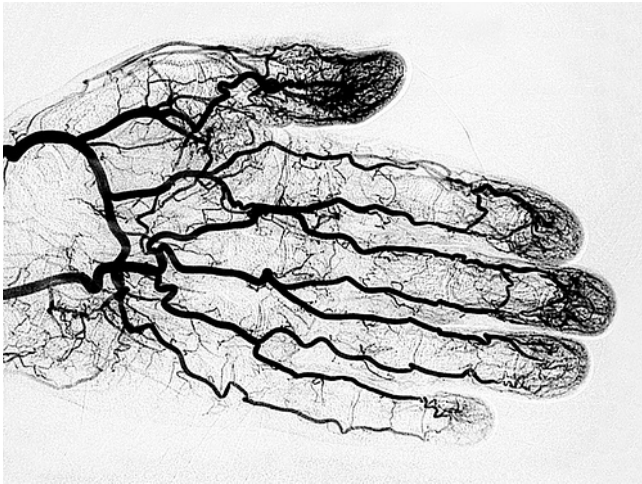

Figure 2.1: Angiogram of the hand [source unknown]

2.1.1 Finger properties

There are probably several properties of the finger which can influence the quality of the captured vascular pattern image, a few of these properties are listed below.

- Creases
- Callous
- Wrinkles
- Wounds
- Blood flow
- Age
- Skin colour
- Fat
- Handedness

Despite the fact of virtually no literature about the effect of these factors on the vascular image quality, a few remarks will be made about these factors. For a full understanding of these factors on the vascular image quality more research is needed.

People doing long-time physical labour will build up more callous on hands and fingers. As a consequence of this blood vessels will lie deeper under the skin surface, which will make imaging these vessels harder. Deep creases can also be of influence, for example a ridge will probably light up more than an edge.

Fresh wounds and scar tissue can probably also have an influence on the captured vascular image. During the healing process more blood is circulated through the hurt area. The paper by Dai et al. mentions that the vessels in the hurt part of the finger are hardly visible [3].

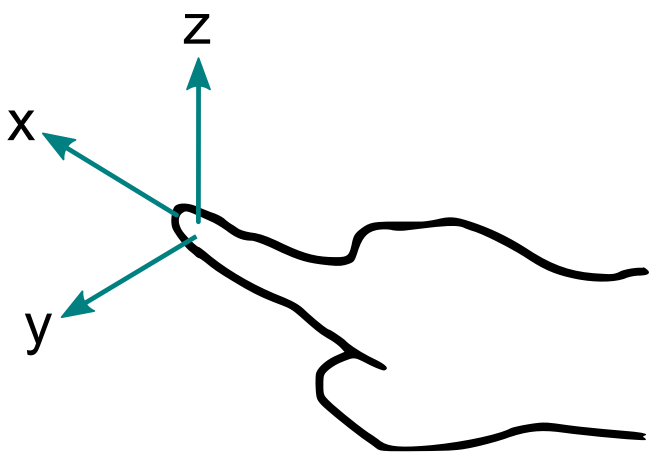

Figure 2.2: Object coordinate system of finger vascular biometrics (modified version [16])

The amount of blood flowing through the finger might also be of influence to the captured image. The factors which have influence on the amount of blood flowing through a vessel include temperature, physical effort, alcohol usage, gender and age.

Elderly people tend to have more wrinkles on their fingers which might cause unwanted shadows in the captured image. Handedness might also influence the captured images, for example images captured of the right hand of a right-handed person might be worse than images captured from his left hand.

For a useful biometric authentication method the biometrics should not change significantly over time. It is still not certain if vascular patterns are time-invariant. The uniqueness of the vascular pattern of the finger was studied by Yanagawa et al. and they conclude that the uniqueness is similar to iris patterns and that finger vascular patterns can be used for personal identification [30].

2.1.2 Anthropometry of the finger

For the design of the imaging device it is important that the majority of the people can use it. Therefore a few anthropometric values have been collected from various sources which can be seen in Table 2.1.

2.2 Imaging device

There is little literature available about the design of an imaging device for capturing vascular pattern images of the finger as it is considered as a side issue by most papers. This section will start by providing an overview of the possible types of imaging devices. Furthermore the light source and camera are treated later on in this section.

source	description of measurement	set percentiles 5%	50%	95%
AWE108 [10]	length	64	73	80
	breadth, proximal	16	20	24
FAA [1]	length (male)	64	74	82
	breadth (male)	19	21	23
	length (female)	62	69	76
	breadth (female)	16	18	21
DINED82 [23]	length (male)	70	78	86
	breadth (male)	17	19	21
	length (female)	63	70	77
	breadth (female)	13	15	17

Table 2.1: Anthropometric measurements of the index finger in millimetres

2.2.1 Types of imaging devices

The white paper by Hitachi [6] mentions three methods for capturing vascular images of the finger. These three methods are presented in Figure 2.3.

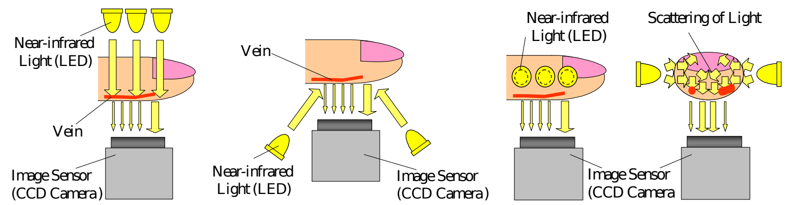

(a) Light transmission (b) Light reflection (c) Side lighting

Figure 2.3: Three methods for capturing vascular pattern images of the finger [6]

The light transmission method places the finger between the sensor and the light source. This method will produce the best images as the light is shone directly through the finger and background light does not have a big influence on the result. The downside of this method is that the user has to stick its finger into the unknown which can be a psychological barrier. The other two methods are not affected by this psychological barrier as the user can see where his finger is placed.

The light reflection method places the light source and the image sensor on the same side of the finger. The image sensor captures the light reflected by the finger. The strong reflection from the skin its surface and the shallow penetration of light under the skin causes the images contrast to be weak [6].

To circumvent the problems of the light reflection method and to have an open sensor the side lighting sensor was proposed. This sensor places the light source on both sides and the sensor beneath the finger. This method will produce better images than the light reflection method.

Most papers use the light transmission mode [3, 8, 13, 25]. There was one paper by Yu et al. which used the side lighting method [33].

Parameter	L810-06AU	SMT780
λ_{peak} $[nm]$	810	780
half width $[nm]$	35	35
total radiated power $[mW]$	22	20
radiant intensity $[mW \cdot sr^{-1}]$	170	6.5

Table 2.2: Parameters of LEDs, 50 mA forward current

Sony has recently put a finger vascular pattern device on the market which uses a form of side lighting. Instead of illuminating both sides of the finger only one side of the finger is illuminated. The advantage of this method is that the finger can directly be placed on the light source. The downside of this method is that the captured vascular pattern image is more subjective to roll around the x-axis of the finger. The roll effect can possibly be compensated for by aligning the vascular image.

Another method for capturing the vascular pattern of the finger is by using some line scanning device. The advantage of this method is that imaging device can be reduced in size. At the moment of writing no such devices exist, and is not mentioned in any published papers.

2.2.2 Position of finger

For template matching it is important that the finger in both images have the same orientation and location. Possible orientation differences are caused when there is a slight roll around the x-axis of the finger or a rotation in the xy-plane. This orientation can be extracted from the captured image or by the imaging device during the capturing process. For determining the orientation and position of the finger a touch sensor can be used on which the tip of the finger is placed. This method is described by Hitachi in one of their patents [5].

In most sensors the tip is used to support the finger when using the imaging device, having as a consequence that the tip is not captured in the image. This does not matter as the vascular pattern in the tip is too dense to capture clearly.

2.2.3 Light source

The wavelength of the light source should be chosen such that the contrast between tissue and blood vessels is the largest. The most common light source for imaging devices are LEDs, though also laser light can be used [12]. The absorption spectra of water, oxygenated- and deoxygenated haemoglobin can be seen in Figure 2.4. Because both blood vessels carrying oxygenated blood and deoxygenated blood must be visible in the captured image, the chosen wavelength for illumination must not discriminate between the two. The figure shows that the wavelength range suitable for capturing the vascular pattern of the finger lies somewhere between 800 nm and 1000 nm. The wavelengths of the LEDs used in existing literature vary from 780 nm to 890 nm [25, 33] but the most common wavelength seems to be 850 nm. LED types such as the L810-06AU, produced by Epitex and the SMT780 produced by Marubeni Corporation are used [13, 25] as light source in current literature.

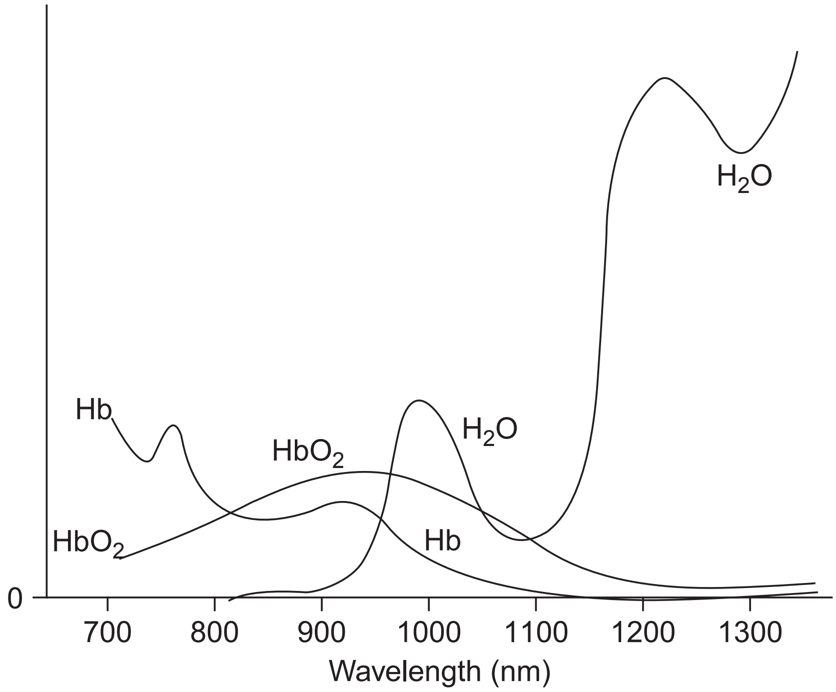

Figure 2.4: Absorption spectra for oxygenated haemoglobin (HbO_2), deoxygenated haemoglobin (Hb) and water (H_2O) (modified version [26]).

A problem which occurs when capturing images is that the brightness within and across images may vary. The brightness within an image may vary because the finger is not equally thick everywhere. The brightness may also vary across images due to variations in finger size and background light. For experimental purposes the current level of the LEDs can be adjusted manually [13]. For practical purposes non-uniform lighting can be used [3]. This non-uniform lighting is realised by analysing the captured image and sending feedback to the light controller which will adjust the output power of the LEDs individually.

Safety

Working with high-power infrared LEDs might induce some safety regarded issues. Their are many standards related to working with non-coherent optical radiation. One of them is the European Union directive 2006/25/EC [4]. This standard is based on the recommendations of the International Commission on Illumination (CIE) and the European Committee for Standardisation (CEN). The directive mentions two kinds of potential hazard, the first danger is thermal damage of the skin and the second danger is thermal damage to the eye. The damage to the eye can further be divided into damage to the cornea and lens and retina. A study done by Mulvey et al. regarding safety issues in eye-tracking did not find any risk of using infrared light [24]. The study does not address the issue of long term exposure to infrared light.

2.2.4 Camera

Each of the setups mentioned in the literature makes use of a near-infrared filter to block out visible light reaching the camera. The size of the captured images range between 320×240 pixels to 640×480 pixels [25, 13]. The resolution of these images is not known. The most common image format for storing the captured images is by using an 8-bit grey scale. Examples of cameras used to acquire the images are the SV1310FM CCD camera produced by Daheng Image and the NC300AIR produced by Takenaka Systems [3, 13].

The image quality is important for further processing. The requirements for a good image depend on the algorithm used for feature extraction. Possible requirements can be total vessel length, number of bifurcations and the standard deviation of grey values [3].

2.2.5 Commercial products

At the moment of writing Hitachi is the leader in finger vascular pattern authentication devices. Figure 2.5 shows some of the finger vascular pattern authentication products produced by Hitachi and Sony. The two devices on the

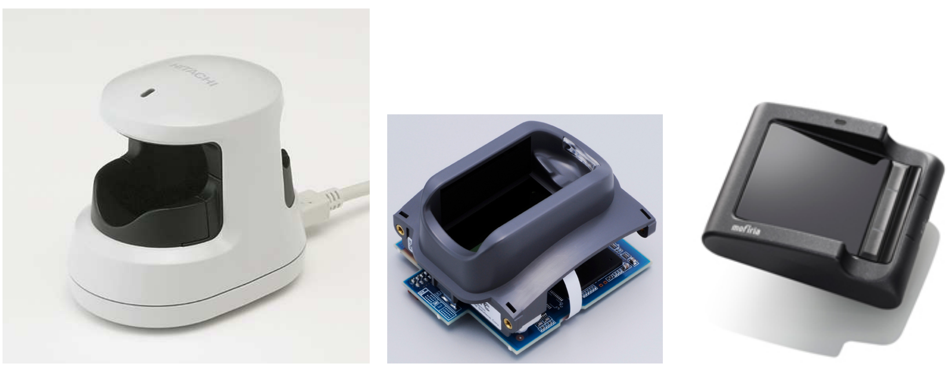

(a) H1 Unit (b) TS-E3F1 (c) FVA-U2SX

Figure 2.5: Commercial finger vascular pattern products

left are both produced by Hitachi. The brochure of these products mention a similar performance for both products, both claim a FRR of 0,01% and a FAR of 0,0001%. The figure on the left shows a USB based logical access reader, the Hitachi H1 unit. This device makes use of the light transmission method. The device was tested according to the ISO/IEC 19795-1 standard.

The figure in the centre shows the TS-E3F1 finger vascular patten sensor produced by the Hitachi-Omron Terminal Solution cooperation. This device probably makes use of the side-lighting method. The performance of this device has been evaluated by the International Biometric Group in 2006 [9]. For the attempt-level performance using 'both instances' they reported an EER of 1.33% for same-day performance and an EER of 2.29% for different day performance.

Sony has also started with finger vascular pattern authentication technology which they have dubbed 'mofiria'. In 2009 they released their first product, the FVA-U1. A later device called the FVA-U2SX can be seen in Figure 2.5c. The lighting method is the single-sided lighting method. No performance figures of this device are known.

A downside for some applications which want to use the finger vascular pattern as biometric authentication method is the size of the imaging devices, these are still quite large. For example mobile devices such as laptops or smartphones cannot use this technology yet. Recently Hitachi has announced an imaging device which is just 3 mm thick and has potential to be used in mobile devices [7].

2.3 Algorithms

This section will try to summarise the various methods of pre-processing, feature extraction and matching. The last section assesses the performance of various algorithms.

2.3.1 Contour extraction

For some algorithms it is important to extract the contour of the finger. The shape of finger contour contains information about the finger geometry which can also be used as an extra biometric feature to increase the performance. A possible method to extract the finger contour is to use separate masks for extracting the upper and lower contour [11, 16]. Another simple method would be to take the directional derivative in the y-direction [13]. A more complex method is to use active contours and curvature estimation [8].

2.3.2 Alignment

Another step which is done often is alignment of the image, this is often necessary because the orientation of the finger can differ slightly between captured images. Possible orientation differences are caused by movement in the xy-plane or by a slight rotation of the finger around its x-axis. To compensate for these orientation differences the extracted minutia points of the binarised and thinned vascular pattern can be used to determine a suitable affine transformation [16] for aligning the captured image with the template image. To determine the movement in the horizontal plane a least square method can be used to estimate a straight line through the centre of the finger contour [16]. The properties of this line can be used to transform the image such that the centre line is in the centre of the image. To compensate for the rotation of the finger the assumption can be made that the cross-section of a finger resembles an ellipse. Using this assumption an elliptic transformation can be determined to align the image [16]. To align the finger position in the horizontal direction is difficult as in most cases the position of the fingertip is not visible in the image. The tip is usually placed on some supporting structure, this is probably the reason that Hitachi has placed some kind of touch sensor in the supporting structure. Another possible solution for normalizing the finger position in the horizontal direction is by using the distal interphalangeal joint. The density of synovial fluid filling the clearance between two cartilages is much lower than that of bones which means that the joint will be visible as a brighter area in the image [31].

2.3.3 Pre-processing

The pre-processing of the acquired image plays an important role in feature extraction. A common step is the removal of noise from the image, this can be done by using a low-pass filter [25, 13, 28]. A better approach would be to use an edge-preserving filter for removing noise [27]. Another pre-processing step which is done often is to downscale the captured image [25, 8]. This downscaling will save computation time, but the downside is that information might be lost. Another pre-processing step which is done often is histogram equalization [25, 27, 14]. This is done to compensate for varying light intensities in the captured image. A common pre-processing step which is often done is image restoration, the goal of this is to enhance the veins in the image. An interesting approach for image restoration is by using an estimated point spread function [17].

2.3.4 Feature extraction & matching

Probably the most simple method of verification is to determine the similarity between a reference image and an input image using the correlation coefficient [13].

A pre-processing step which is often done is adaptive thresholding [11, 33, 25]. After this step a skeleton image can be produced using a thinning algorithm. From this skeleton image line endings and bifurcations can be extracted as unique features. As a similarity score between a reference and an input image the modified Hausdorff distance can be used [11].

The adaptive thresholding step can also be followed by a simpler thinning approach which makes use of a median filter for smoothing the image. After this template matching can be used for identification [25].

Another method of feature extraction is by using line tracking algorithms [22, 8]. After this matching can be done by template matching or an extra step can be performed which normalises the pattern. This pattern normalization model is based on two assumptions: the finger its cross section has an elliptical shape and the blood vessels being imaged are close to the surface [8]. This paper concluded that the extra normalization step improves the performance.

A combination of adaptive thresholding and line tracking can be used to achieve better results [33].

A relatively unique approach for extraction features is described by Wang et al. [28] They suggest using a Radon transform and singular value decomposition (SVD).

2.3.5 Performance overview

A summarising table with the performance mentioned in some of the papers is given in Table 2.3. The most common performance figures mentioned are the false acceptance rate (FAR) and the false rejection rate (FRR). The equal error rate (EER) is the rate at which the FAR and the FRR are equal to each other. The mentioned EER of the various algorithms range from 1,164% up to 0,0009%. The table also mentions the number of unique volunteers (*u persons*), the number of fingers captured per volunteer (*fingers/person*), the number of unique fingers captured per volunteer (*u fingers*), the number of images captured per finger (*images/finger*) and the total number of captured images (*total*).

Authors	Year	Method	u persons	fingers/person	u fingers	images/finger	total	EER [%]
Kono et al.[13]	2002	normalised cross-correlation	678	1	678	2	1356	0,00
Miura et al.[22]	2004	repeated line tracking	678	1	678	2	1356	0,145
Miura et al. [21]	2005	maximum curvature	678	1	678	2	1356	0,0009
Zhang et al. [34]	2006	multiscale, curvelets	400	8	3200	1	3200	0,128
Lee et al. [16]	2009	local binary patterns	60	8	480	10	4800	0,081
Lee et al. [18]	2009	restoration, skeletonisation	80	8	640	10	6400	0,76
Choi et al. [2]	2009	principal curvature	?	?	29	?	118	0,36
Huang et al. [8]	2010	wide line detector	5208	1–4	10140	5	50700	0,87
Wang et al. [28]	2010	radon transform	10	1	10	10	100	0,01
Kang et al. [11]	2010	skeletonisation	102	8	816	10	8160	1,164
Lee et al. [15]	2011	local derivative pattern	30	8	240	10	2400	0,89

Table 2.3: Performance of several algorithms used for finger vascular patterns biometrics

A note of scepticism should be added to the mentioned performance figures. In general the procedure of capturing is not clear, for example most papers do not mention whether the images captured per unique finger are collected in one session or are captured over time. All the papers mentioned in the table lack uncertainty measures for their results, which is a pity. The total number of vascular images in correspondence to the mentioned performance is by all means questionable. For example, determining an EER of 0,0009% with high certainty is not possible with the mentioned number of 1356 images. Huang et al. [8] have tested the algorithms proposed by Miura et al. on their collected data. With normalization they achieved an EER of 2,8% for the maximum curvature method and an EER of 5% for the repeated line tracking method. Choi et al. have also done a verification of the maximum curvature method and they have achieved an EER of 3,58%. Kumar et al. [14] have also verified the performance of Miura's maximum curvature and repeated line tracking method. They achieved an EER of 8.25% for the repeated line tracking method and an EER of 2.65% for the maximum curvature method. The mentioned EER's are the average of the middle and index fingers.

Another example of a questionable performance figure is the one mentioned by Wang et al. [28], capturing ten vascular images from ten volunteers is by no means enough to determine this EER. Another questionable fact is the usage of one image per finger which is done by Zhang et al. [34]. If only one image is captured per finger it would not be possible to determine a false rejection rate.

The performance of finger vascular pattern biometrics can be further improved by combining it with other biometric features. A feature which is already present in the captured image is the geometry of the finger. For example the paper by Kang et al. has an EER of 1,164% for finger vascular pattern recognition on itself and by combining it with finger geometry the EER decreases to 0,075% [11].

2.4 Datasets

The number of finger vascular pattern datasets available to the research community is low, the properties of the available datasets have been summarised in Table 2.4. The Peking University in China have collected a few of the available datasets. They have three datasets available for research, of which two contain hand-picked images using some unknown criteria.

Another finger vascular pattern dataset has been collected by the Shandong University [32]. The images collected in this dataset look promising but two remarks should be made. First it seems that the time difference between capturing images of the same finger is very small. As if the finger has remained positioned in the capturing device between capturing moments. As a consequence of this no reliable False Rejection Rates can be determined. Another possible issue is the visibility of adjacent fingers in the image. This might make the detection of the finger region difficult or even erroneous.

The last finger vascular pattern dataset found has been collected by the Hong Kong Polytechnic University [14]. The quality of these images is not very good, this might be caused by the fact that a true touch less device has been used to capture the images. One good point of this dataset is its extent and the fact that also an image of the finger is captured in the visible spectrum. Because two types of images are captured the performance of fusing the vascular patten and crease pattern can be examined. The numbers mentioned in the table are for the vascular pattern dataset.

One thing which is missing from all these datasets is some basic meta-information such as gender and age of the participants. Other information missing is the resolution of the captured images. This makes it difficult to compare various algorithms using different databases.

The last row in the table is the dataset which has been collected as part of this research and contains meta-information about the participants.

The finger vascular patten images are generally collected from students at the university. It is questionable how representative a university population is. The population at a university will probably be within a certain age range, consists of a higher number of males and will not perform a lot of physical labour. To collect a truly good dataset the dataset should resemble a cross section of the population.

Name	University	Participants	Fingers p.p.	Tot. fingers	Images per finger	Total	Image size
SDUMLA-HMT	Shandong University, China	106	6	636	6	3816	320×240
Finger Vein Database (V4)	Peking University, China	?	?	200	4–8	1528	512×384
Finger Image Database (V1)	Polytechnic University, Hong Kong	158	2	316	12	3744	513×256
UT dataset	University of Twente, Netherlands	59	6	354	4	1416	672×380

Table 2.4: Various finger vascular pattern datasets available

The International Organization for Standardization (ISO) specifies an image format for exchanging vascular image data. The specifications have been recorded in the ISO/IEC 19794-9:2011 standard. The main purpose of this standard is to define a data record format for storing and transmitting vascular biometric images and certain of their attributes for applications requiring the exchange of raw or processed vascular biometric images [19].

2.4.1 Test size

This section is based on the report *Biometric Testing Best Practices, Version 2.01* written by Mansfield, A.J. and Wayman, J.L. [20]. Lower bounds to the number of attempts needed for a given level accuracy can be determined by rules such as the "Rule of 3" and the "Rule of 30". An example for both rules will be provided, assuming that an EER of 1% can be reached. As the information provided in this section is very concise the reader is urged to read the mentioned document.

Rule of 3

The "Rule of 3" for a 90% confidence level is as follows:

$$p \approx 2/N \tag{2.1}$$

In this equation p is the error rate for which the probability of zero errors in N trials purely by chance is 10%. With the made assumption of an EER equal to 1% this will lead to 200 trials. If there are zero errors in these 200 trials it can be said with 90% confidence that the error rate is 1% or less.

Rule of 30

The "Rule of 30" states that to be 90% confident that the true error rate is within the ± 30% of the observed error rate, there must be at least 30 errors. So, for example, if we have 30 false non-match errors in 3,000 independent genuine trials, we can say with 90% confidence that the true error rate is between 0.7% and 1.3%.

Chapter 3

Sensor design

This chapter will focus on the design of a sensor capable of capturing vascular pattern images of the finger. The objective is to design an imaging device which is capable of capturing vascular pattern images of the ring, middle and index finger of both hands. The thumb and pink will not be included as they differ to much in shape compared to the other three fingers. Another reason for not including the thumb and pink is that they are not interchangeable with the other three fingers when determining the performance.

The first section will focus on the results of a few preliminary experiments which are performed prior to designing a sensor. These preliminary experiments are done to get an affinity with the various technological aspects involved when designing a sensor. The next section provides detailed information about the hardware of the sensor. The most important part of the sensor, the transillumination procedure is covered next. The section concludes with some remarks about the realised sensor.

3.1 Prototyping

Before the actual sensor is designed some preliminary experiments are done to get an affinity with the various technological aspects involved. The first aspect investigated is the light source. This is followed by a mock-up of the sensor and a small experiment to try the side lighting method. The last section describes the results obtained from the pilot data collection.

3.1.1 Light source

To determine which wavelength can be used best to capture the vascular pattern of the finger various wavelengths have been tested. From the literature study it is already known that the optimal wavelength should lie somewhere between 800 nm and 900 nm. Several wavelengths have been tested by placing an infrared LED behind the finger and capturing the vascular pattern image with a camera. The results can be seen in Figure 3.1. The index finger of the left hand has been used and the light source has been placed on the distal joint. As it can be seen the difference between the images is not very big. The following LEDs have been used to illuminate the finger: the JET-800-10, the FL850-03-80 and the

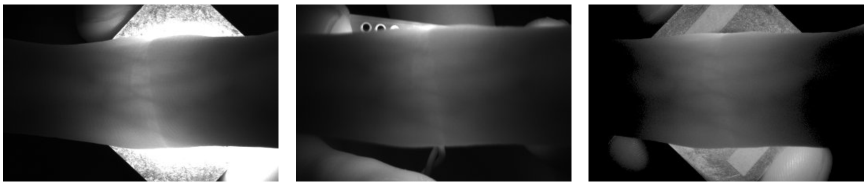

(a) 800 nm (b) 850 nm (c) 870 nm

Figure 3.1: Vascular pattern images captured using various wavelengths

JET-870-05. The wavelengths of these LEDs were 800 nm, 850 nm and 870 nm respectively.

It is difficult to compare the images made using these three different light sources because they do not only differ in wavelength but also in other aspects such as half angle.

The camera used to capture the images of the vascular pattern is the ARTIST camera produced by art innovation. The camera is capable of capturing images within several different spectral bands. In this case the infrared-1 band was used which ranges from 700 nm to 1000 nm.

3.1.2 Mock-up

Before the final imaging device is designed a mock-up has been made. The setup of the mock-up can be seen in Figure 3.2. The camera used is the BCi5 monochrome CMOS camera with a firewire interface produced by C-Cam technologies. The camera has been fitted with a Pentax H1214-M machine vision lens with a focal length of 12 mm. On top of the lens a B+W 093 infrared filter is screwed on.

Eight LEDs have been fitted in a wooden u-shaped frame, which had been painted black on the inside to avoid reflections. The width and the height of the inside of the u-shape was approximately 27 mm and the length of the u-shape was 80 mm. The LEDs are of type TSFF5210 and are produced by Vishay. The LEDs have a peak wavelength of 870 nm and have a typical radiant intensity of 180 $mW \cdot sr^{-1}$. This u-shaped frame is taped on a sheet of 3 mm thick plexiglass. The finger being imaged is placed inside this u-shape. The LEDs are controlled using a custom made light controller which can be controlled using Matlab. During preliminary experiments if was evident that using a flat surface for resting the finger was not desirable. If the finger was pressed against the flat surface the location of the vessels change within the finger and light is guided via the finger to the imaging surface. The effect of pressure can be seen in Figure 3.3. The figure on the left shows a finger with no pressure applied and the figure on the right shows an image in which the finger has been pressed hard on the imaging surface. It can be seen that places with more pressure applied have a higher intensity. Several people were asked to place there finger in the u-shape and soon it became evident that the chosen dimensions were too small.

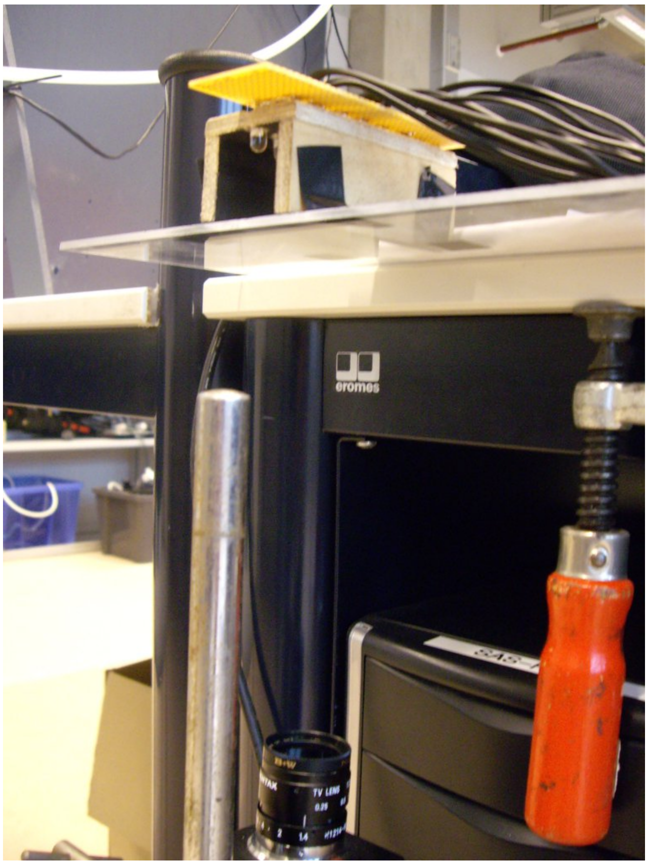

Figure 3.2: Mock-up of the finger vein sensor

3.1.3 Side lighting method

Also a mock-up has been made to test the side lightning method as this is more user friendly. It is more user friendly because the user can see where he places his finger. The mock-up can be seen in Figure 3.4a and a sample vein image produced with this mock-up can be seen in Figure 3.4b. The camera can not be seen in the figure, but it is the same one as in the previous mock-up. As it can be seen from the image the sides of the finger are over exposed. A possible solution to this problem of over exposure is by illuminating the finger sides separately, and combining both images later to form an image without over exposure.

3.1.4 Pilot

Taking the points noted in the preliminary work into account a sensor was designed and tested during a pilot. Details about the pilot can be found in Section 4.1. During the pilot it became clear that the capturing device should accommodate for shorter fingers. Also the top plate was not large enough, part of the ceiling was still visible in the captured images. Another finding was that the finger being captured was not in the centre of the camera view point. One of the problems occurring with the sensor was that if the fingers were placed

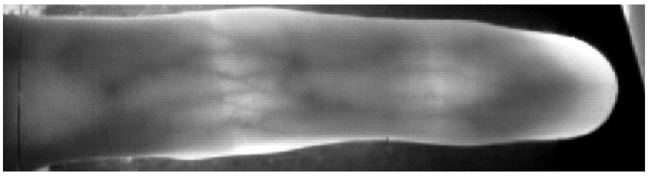

(a) No pressure

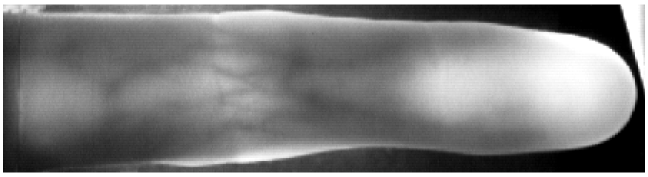

(b) Applied pressure

Figure 3.3: With and without pressure on the imaging surface

Parameter	TSFF5210	SFH4550
λ_{peak} $[nm]$	870	850
half width $[nm]$	40	42
total radiant flux $[mW]$	50	50
half angle $[deg]$	±10	±3
radiant intensity $[mW \cdot sr^{-1}]$	180	700

Table 3.1: Parameters of LEDs, 100 mA forward current

on the sensor the adjacent finger could be visible in the image 3.5b. This can lead to two kinds of problems, the first is the fact that extracting the finger contour is more difficult and the second is that the light which is reflected from the adjacent fingers can disturb the finger being imaged.

The light source used in the sensor are near-infrared LEDs. Two different types of LEDs have been tested, one with a wavelength of 870 nm and the other with an wavelength of 850 nm. The parameters of these LEDs have been summarised in Table 3.1. The difference between the captured images when using one of the two different wavelengths is minimal. Figure 3.6 shows the difference between the two LEDs. For this image the output power per led has remained the same. The only difference is the brightness of the image, this caused by the difference in half-angle between the LEDs. The 850 nm LED has a smaller half-angle and hence less power is needed to transilluminate the finger.

3.2 Final sensor design

After the pilot a few minor adjustments are made to the sensor. The sensor now supports smaller fingers and has a new top plate fitted which covers the hole completely. Also the camera has been adjusted such that the area of interest is in the centre of the captured image. The motivation for choosing the transmission type of sensor is its simplicity and robustness. Another advantage of this type of sensor is that external light conditions have little influence on the captured

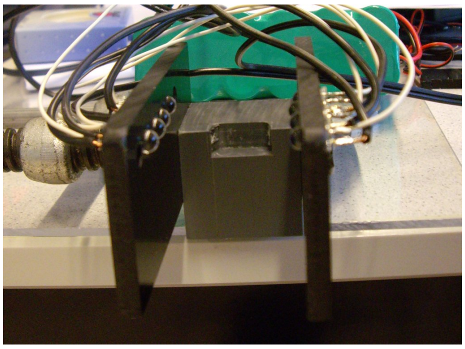

(a) Mock-up

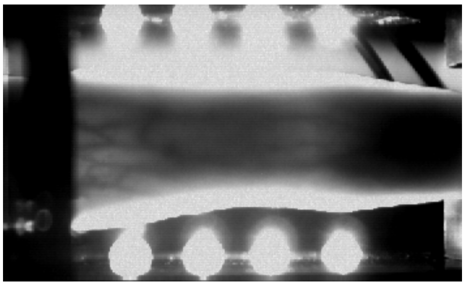

(b) Result

Figure 3.4: Mock-up and result for side lighting

images. The sensor has been build half-open such that the user can see where his finger is placed. To minimise the height of the imaging device a mirror will be used to place the camera in the horizontal plane. The inside of the sensor is made dull by roughening the surfaces to avoid unwanted light reflections. The light control unit has been designed by the technical staff at the research group and can be controlled easily from within Matlab. The camera used in the sensor is the BCi5 monochrome CMOS camera with firewire interface produced by C-Cam technologies. The camera has been fitted with a Pentax H1214-M machine vision lens with a focal length of 12 mm. The lens is fitted with a B+W 093 infrared filter which has a cut off wavelength of 930 nm. The camera is used in 8 bit mode with a resolution of 1280×1024 pixels. The brightness of the camera is set to 75 and the shutter is set to 40. The LEDs have been placed on an interchangeable module, now it is easy to switch between various light sources. The sensor can be seen in Figure 3.7 and details about the dimensions of the sensor can be found in Appendix B.1.

The mirror which is used to bend the path of light by 90° is the NT41-405 mirror from Edmund Optics. This is a first surface mirror, which means the reflective layer is deposited directly on one surface of the glass substrate. The advantage of this is that the path of light does not need to pass through glass before reaching the reflective surface. A downside of this type of mirror is that the surface is prone to oxidation and scratches. The reflective coating on this mirror is enhanced aluminium which has a good reflectance in the visible range but in the near-infrared part of the spectrum it has a reflectance of roughly 85%. The images captured by the sensor are 672×380 pixels and have a resolution of

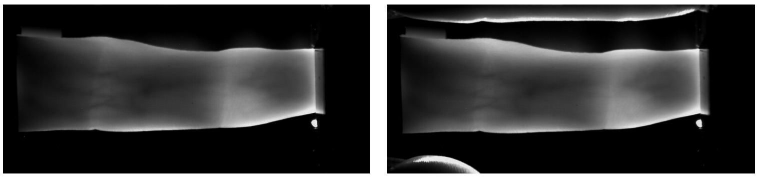

(a) Normal image (b) Image with adjacent fingers

Figure 3.5: Problem occurring with extra fingers

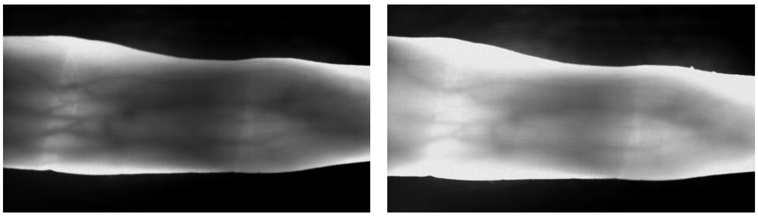

(a) TSFF5210 - 870 nm (b) SFH4550 - 850 nm

Figure 3.6: Difference between the two LED types

126 pixels per centimetre (ppcm). In non-metric units this would be 320 pixels per inch (ppi). The format which is used to store the images is 8-bit grey scale PNG, which is a lossless format.

3.3 Transillumination procedure

Each of the intensities of the eight individual LEDs can be controlled separately. This is useful as the thickness of the finger differs between persons and across a single finger. In general the tip of the finger is smaller then the base of the finger. In order to make the feature extraction easier it is beneficial to have a uniform intensity across the whole finger. This uniform intensity can be realised by adaptively controlling the intensity of the LEDs using some kind of control loop.

In order to design such an algorithm first the relation between LED intensity and grey levels in the image must be investigated. This investigation is done by increasing the intensity of each LED and measuring the average grey level directly underneath the corresponding LED. An area of ten by ten pixels was used to determine the averages. Figure 3.8 shows these relations. The eight measurement positions are directly under the LEDs. The first measuring position is at the finger tip and the last measurement position is at the base of the finger. It can be seen that the relation between the LED intensity and the mean grey level is approximately linear. The curves corresponding to measurement position one and two, which are at the tip of the finger, shows the largest gradient. The gradient at measurement position seven is surprisingly high as well, this is because the LED is situated directly above the distal interphalangeal joint.

A very simple method to determine the intensities of the individual LEDs would be to switch them on one by one and increase the intensity until the mean

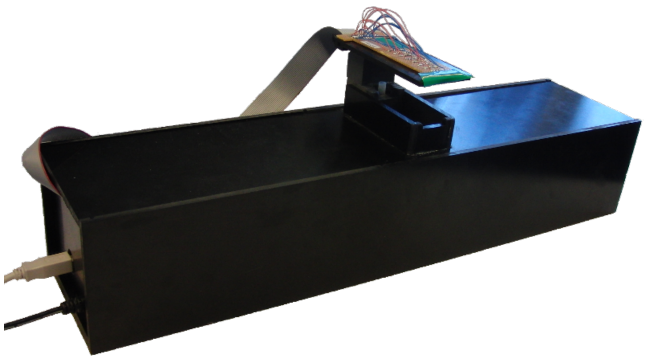

Figure 3.7: Final sensor

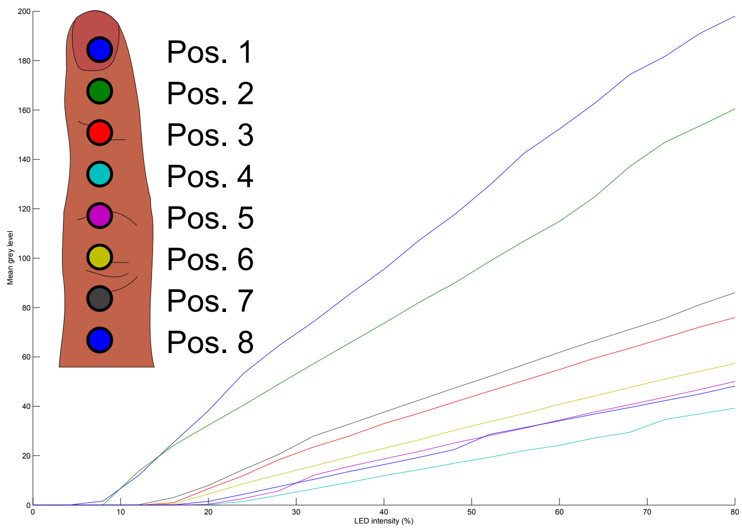

Figure 3.8: Mean grey levels versus LED intensities

grey level under the LED falls within a specified range. A flowchart of this simple control loop is given in Appendix B.2 together with the parameters used.

A downside of this method is that at the end the image intensity decreases. This can be seen in Figure 3.9. For example when adjusting the LEDs from left to right, the image intensity at the right of the image will be lower as it has no neighbours which contribute to the mean grey intensity value at the specified measurement point. To compensate for this effect the LEDs can be adjusted from the edges to the centre which leads to an image with a more uniform intensity. This method is used during the collection of the real database.

Two other methods for controlling the intensity per LED have also been investigated. The first method was based on determining the width of the finger which is assumed to be proportional with the thickness of the finger. The second method was based on the linear relation between the intensity and grey level value. By increasing the intensity of the LEDs one by one it was possible to determine a transfer matrix which relates the LED intensity to the mean grey level values. In theory it would be possible to determine the LED intensities

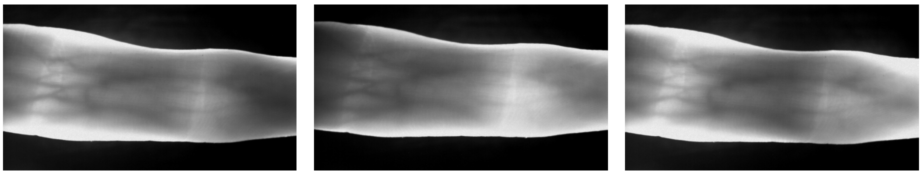

(a) Left to right (b) Right to left (c) Outward to centre

Figure 3.9: Adjustment directions

by taking the inverse of this matrix and multiplying it with the desired mean grey level value. A downside of this method was its speed, determining this transfer matrix took a long time. The parameters of this linear relation can be estimated by extrapolating the values obtained from a small number of sample points. This might increase the adjustment speed of the algorithm.

3.4 Final remarks

Instead of using a mirror with an enhanced aluminium coating it might have been better to use a mirror with a protected gold or a protected silver coating. These types of coatings have a better reflectance in the near-infrared part of the spectrum. It might also be better to use a filter which has a lower cut-off frequency. In this case the cut-off frequency is 930 nm which means that some of the light is still absorbed by the filter.

Chapter 4

Data collection

This chapter will be provide an overview of the two data sets collected. The first data set collected was part of a pilot study and comprises a small number of volunteers. During the pilot the effect of external conditions which might effect the visibility of the vascular pattern in the captured images is investigated. The second data set collected is for publication and a consists of a large number of volunteers. The fingers in both datasets are numbered according to Figure 4.1.

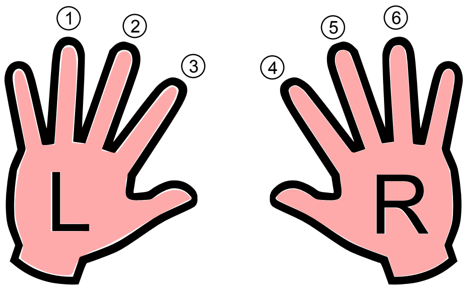

Figure 4.1: Numbers associated with the fingers

4.1 Pilot

Before a large dataset is collected a pilot is done consisting of a small number of volunteers. The objective of this pilot is to detect any teething problems and to investigate the effects of temperature and stress on the captured vascular pattern. The goal is to collect data from at least ten volunteers. For each volunteer the vascular pattern of the index, ring and middle finger from both hands will be collected. The meta-information recorded will be the gender, age and handedness of the volunteers. The pilot will consist of two identical sessions separated at least by two weeks.

During each session four measurements will be made. Each measurement will consist of all six fingers being captured, starting with the index finger of the left hand. The total number of images captured per volunteer during these two sessions will be 48. The first two measurements done within a session will be a normal one, no external conditions will be applied. For the third measurement the volunteer will be asked to operate a finger muscle training device, which can be seen in Figure 4.2, for thirty seconds. To operate this device a firm grip is needed to squeeze the handles towards each other. The training with this device will be done for each hand separately. After operating the training device the

Figure 4.2: Finger training device

vascular pattern images will be captured from the corresponding hand. This procedure is also repeated for the other hand. For the last measurement the volunteer will be asked to submerge his hand in a large container filled with ice-cold water for thirty seconds. The step-wise measurement procedure has been summarized below.

1. Capture all six fingers of both hands
2. Capture all six fingers of both hands again
3. Train left hand for 30 seconds using apparatus
4. Capture all three fingers of the left hand
5. Train right hand for 30 seconds using apparatus
6. Capture all three fingers of the right hand
7. Submerge left hand in ice-cold water for 30 seconds
8. Capture all three fingers of the left hand
9. Submerge right hand in ice-cold water for 30 seconds
10. Capture all three fingers of the right hand

For each volunteer a separate directory with a unique id will be created containing all captured images from both sessions. The following filename format will be used for storing the captured images:

`{measurement_id}_{finger_id}_{date}-{time}{.png}`

For example the file `2_4_120130-104657.png` belongs to the right hand index finger and has been captured during the second measurement on 30^{th} of January 2012 at 10:46:75. The data collected during the pilot is not available for the public as the participating volunteers did not sign any consent form.

Age	Frequency
24	2
25	1
26	1
27	2
29	1
30	1
48	1
55	1
56	1

Table 4.1: Frequency table of participants age in the pilot

4.1.1 Realisation

A total number of eleven volunteers participated in this pilot of which eight were male and three were female. All of the volunteers were right handed and the age of the volunteers varied between 24 and 56, details about age are given in Table 4.1. The number of days between the two measurements sessions ranged from fourteen to fifteen days.

To test the effects of temperature on the vascular pattern of the finger a container with ice-cold water was used. The ice-cold water had a temperature which varied between 5 to 8 °C. Submerging the hand into this ice-cold water during thirty second was experienced as rather unpleasant for most volunteers. The size of the captured images was 751×381 pixels. The captured images are stored as 8 bit grey level Portable Network Graphics (PNG) files. Visible blood vessels in these images are approximately 5 to 20 pixels wide.

The graphical user interface (GUI) used for capturing the images can be seen in Figure 4.3. The GUI shows a graphical representation of the current finger being captured in the upper left corner. The current finger being captured is clearly indicated by the green colour. The top right pane shows a live preview of the camera. When a snapshot is made the image is shown in the bottom right pane. The operator can judge the captured image before saving the image to disk.

4.2 Dataset collection

This section will describe the process of collecting a large set of vascular pattern images for publication to the research community. Prior to contributing to the dataset volunteers first had to read a general information letter and sign a consent form. The information letter and consent form are included in Appendix A as a reference. The data is collected during two sessions which are separated by approximately two weeks. This time interval will provide more realistic results as in practice there is also a time interval between enrolment and authentication. In each session all six fingers of the volunteers are captured twice.

The data collected from the volunteers will be processed anonymously by giving each volunteer a unique id. The meta-data collected from the volunteers will be their age, gender and handedness. It was chosen not to record the

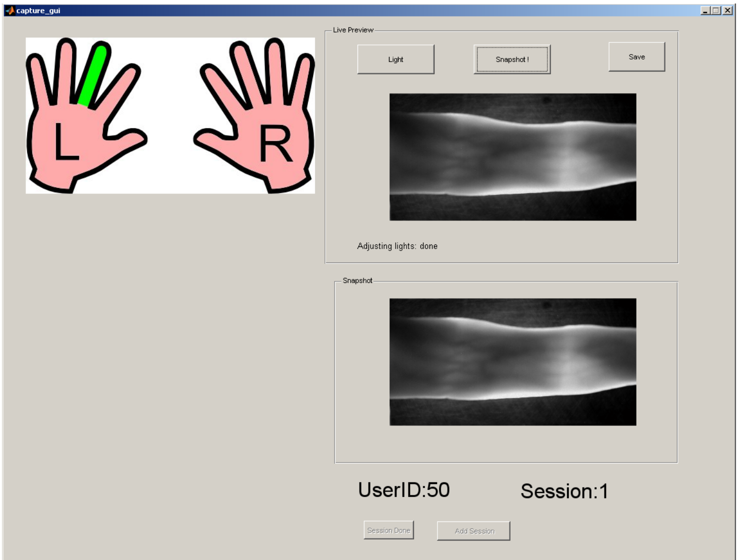

Figure 4.3: Graphical user interface for capturing the vascular pattern images.

ethnicity of the volunteers as this is a delicate subject and it is rather difficult to make clear categories for different ethnicities. Any oddities occurring during the data collection will also be recorded.

The same graphical user interface as in the pilot is used to capture the images. The captured images will be stored using the lossless PNG format. The ISO/IEC 19794-9:2011 standard will not be used as there are no tools available yet to support this format. The filename format for storing the images will be as follows:

`{person_id}_{finger_id}_{measurement_id}_{date}-{time}{.png}`

The reason for including the *person id* in the filename is that it can directly be seen from the filename to which directory this particular image belongs. The reason for mentioning the *finger id* before the *measurement id* is that if the filenames are sorted all images from the same finger will be grouped. For example the file `0028_3_4_120523-112948.png` corresponds to the index finger of the left hand of volunteer number 28. The image was captured during the second measurement round of the second session on the 23^{rd} of May 2012 at 11:29:48.

The following acquisition protocol was followed during the acquisition:

1. Provide introduction
2. Let volunteer read & sign consent form
3. Fill in meta-data if there is no objection
4. Capture all six fingers, starting with finger 1
5. Capture all six fingers again

During the second measurement session steps 1–3 could be omitted of coarse.

	absolute	%
Gender		
Male	44	75
Female	15	25
Handedness		
Left	7	12
Right	51	86
Undefined	1	2
Publishable		
Yes	54	92
No	5	8

Table 4.2: Statistics about the collected dataset.

4.2.1 Realisation

Volunteers were chosen such that the chance of finding them back after two weeks was high. The data collection took place in May 2012. Capturing all six finger twice took about five minutes per volunteer. If adjacent fingers were visible in the live preview, the user was asked to re-position its finger such that the adjacent fingers were not visible in the image any more. In general this repositioning of the fingers was not necessary. A few volunteers still had a little trouble positioning their finger in the sensor due to the limited length of their fingers. Volunteers which wore a ring were asked to remove it if it was visible in the live preview.

During the first session a total number of 60 volunteers participated, after two weeks 59 volunteers participated again. Hence the dataset consists of 59 volunteers which had 4 images captured per finger which leads to a total of $59 \times 6 \times 4 = 1416$ images. Some statistics about gender, age and whether images may be published is summarized in Table 4.2. The table show the absolute number of volunteers as well as the percentage.

The average number of days between the two measurements sessions was 14 days. More details about the number of days between the measurements is given by the histogram in Figure 4.4b. The age of the volunteers ranged from 19 up to 57, with the majority in their twenties and thirties. Details about the age of the volunteers is given by the histogram in Figure 4.4a. The first bin of the histogram corresponds to the ages 16–20, the second bin corresponds to ages 21–25 etc.

Some sample images from the collected dataset can be seen in Figure 4.5. The quality of the collected images vary from person to person, but the variance in quality of the images from the same person does not vary that much. The width of the visible blood vessels range from 4–20 pixels which corresponds to widths of 0.3–1.6 mm.

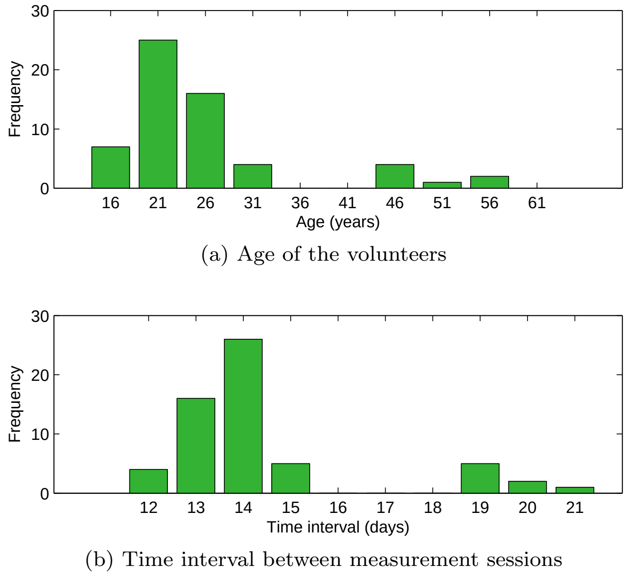

(a) Age of the volunteers

(b) Time interval between measurement sessions

Figure 4.4: Histograms of the age of volunteers and the time interval between measurement sessions

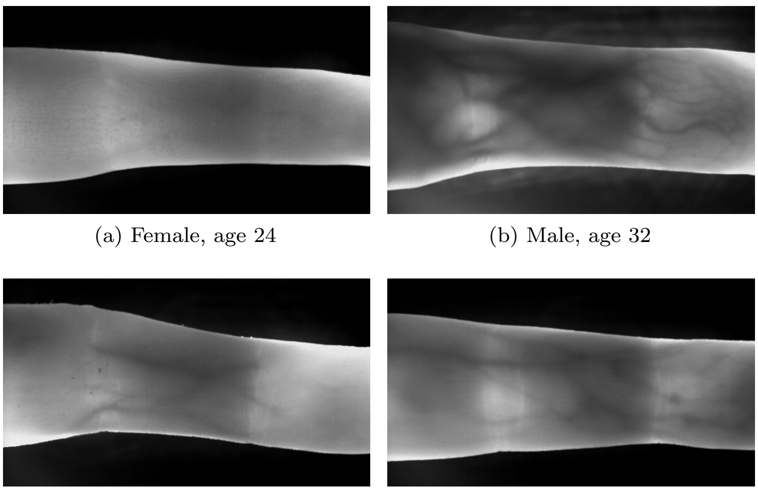

(a) Female, age 24

(b) Male, age 32

(c) Male, age 20

(d) Female, age 31

Figure 4.5: Sample images of the left hand ring finger from the collected dataset.

Chapter 5

Algorithms

In order to verify some of the algorithms mentioned in existing literature the proposed algorithms must be implemented as none of the algorithms were available to the public. Another goal of this testing is to characterise the dataset. This chapter will give an overview of the implemented algorithms and some of the necessary pre-processing steps. In the first section two methods of extracting the region of interest are investigated. After this the next step is normalisation as the finger can be placed in the sensor at different orientations. The third section focuses on one of the common pre-processing steps which is histogram equalisation. The last section treats the various feature extraction methods. All algorithms are implemented using MathWorks Matlab version R2011b.

5.1 Region of interest

One of the key actions during testing is the detection of the finger region. In the work of Kumar et al. [14] it has been proven that using masks the performance increases significantly. Detecting the finger region is not that difficult as the transition from background to finger is abrupt. The finger region detection method used in this research is described by Lee et al. [16]. This method filters the image using a simple mask, at the transition from background to finger this mask will give a large response. The filtered image can be seen in Figure 5.1b. The mask used for filtering this image had a width of 40 pixels and a height of 4 pixels. The white and dark lines correspond to the upper and lower finger edge respectively. For determining the edges the filtered image is divided into

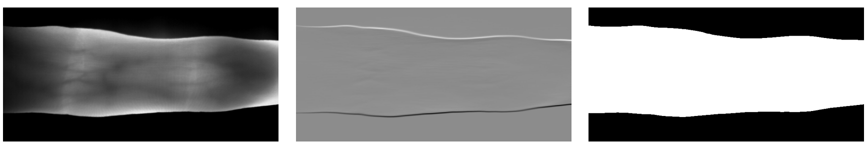

(a) Original image (b) Filtered image (c) Binary finger mask

Figure 5.1: Finger region detection method

two parts, an upper and a lower part. For detecting the upper finger edge the coordinates of the maximum values are used and for detecting the lower edge of the finger the minimum values are used. The area between the detected finger edges is filled to create the binary finger mask. The final detected region can be seen in Figure 5.1c. A downside of this region detection method is that the assumption is made that the upper finger edge is present in the upper part of the image and that the lower finger edge is present in the lower part of the image. This finger region mask is later used to mask the results of various feature extraction methods. The described finger region method is provided by the custom `lee_region()` function.

Also the finger region detection method described by Kono at. al [13] has been implemented. The method is provided by the custom `kono_region()` function. This method is very similar to the one described above. The only difference is that in this case no masks are used but a filter kernel which is sensitive to changes in the y-direction of the image. An advantage of this method is that the detected finger edges are smoother compared to Lee's method.

5.2 Normalisation

Normalisation is important as the orientation of the finger can change between capturing moments. This normalisation ensures that the finger will be aligned to the centre of the image. The normalisation uses the coordinates of the upper and lower detected edges which are returned by the finger region detection method. The normalisation method used in this research is described by Huang et al. [8]. This method attempts to fit a straight line between the detected finger edges. The parameters of this estimated line, a rotation and a translation, are used to create an affine image transformation. The line fitting method used is Matlab its `robustfit()` function, which is part of the Statistics Toolbox. Figure 5.2a shows the detected finger edges in red and the estimated line through the centre of the finger edges in green. The estimated parameters of this specific line are a translation of 27 pixels and a rotation of 8.4 degrees. The normalised image can be seen in Figure 5.2b. The normalisation implementation made for

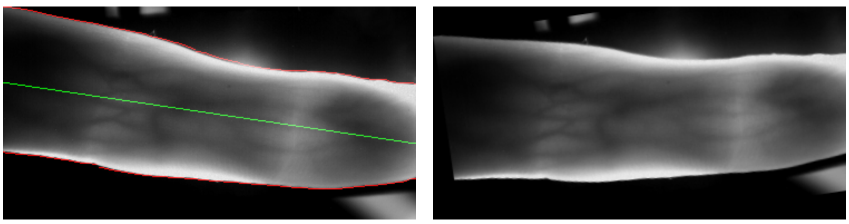

(a) Rotated finger image with edges(red) and fit line(green) indicated

(b) Image after affine transformation

Figure 5.2: Finger normalisation

this research only compensates for rotations in the xy-plane. The mentioned paper also suggests a method for compensating rotations around the x-axis, this method is not implemented though. The normalisation is provided by the custom Matlab function `huang_normalise()`.

The normalisation procedure as described by Lee et al. [16] has also been inspected. This method tries to normalise the finger based on the minutia of the skeletonised vascular pattern. The method tries to find an affine transform such that groups of three minutia are matched between two images. The parameters of the affine transform must fall within certain predetermined ranges. Of all these groups of three minutia points the set of points which results in the smallest average minimum distance is used. During testing it was noticed that it takes a long time to calculate the parameters of all possible combination of three minutia. For example if an image has 17 minutia points and the reference has 15 minutia points the total number of parameter estimates becomes:

$$\binom{17}{3} \times \binom{15}{3} = 309400 \tag{5.1}$$

An advantage of this method is the possible compensation for the rotation around all three axis and the compensation of translation in the x- and y-direction.

5.3 Pre-processing

A pre-processing step which is done often in existing literature is histogram equalisation. Histogram equalisation changes the original intensity values such that a specified histogram shape is approximated. This step can be used to compensate for non-uniform lighting conditions in the captured vascular pattern images. The result of an adaptive histogram equalisation algorithm applied to a vascular pattern image can be seen in Figure 5.3. The adaptive histogram

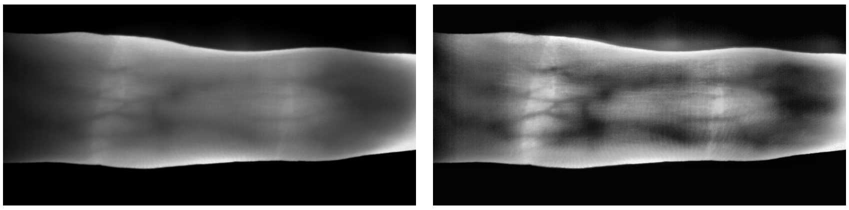

(a) Original image (b) Adaptive histogram equalisation

Figure 5.3: Adaptive histogram equalisation applied

equalisation algorithm is provided by the Matlab its `adapthisteq()` which is part of the Image Processing Toolbox. This function makes use of the contrast limiting adaptive histogram equalisation (CLAHE). The default parameters of this function were used to create the image above. As it can be seen the contrast is enhanced significantly and even some of the creases of the finger become visible. A downside of histogram equalisation is that noise might be enhanced.

5.4 Feature extraction

This section will summarise some of the popular feature extraction methods from literature. The first subsection will treat the normalised cross-correlation, this method is used as a reference performance. The consecutive subsections will look at the other feature extraction methods.

5.4.1 Normalised cross-correlation

In order to get some kind of reference for performance comparison the most basic type of matching method is used, which is a normalised cross-correlation between the reference and the input image. This method has also been used by Kono et al. [13]. The normalised cross-correlation used is provided by the Matlab function `normxcorr2()` which is part of the Image Processing Toolbox. The maximum value of this correlation is used as matching score. In order to calculate a cross-correlation the reference image must be equal or smaller than the input image.

5.4.2 Miura's maximum curvature method

The maximum curvature method for extracting vascular features by Miura et al. [21] is one of the most popular methods of vascular pattern extraction at the moment and was proposed in 2005. This method looks at the local maximum curvature in four directions, the horizontal and vertical directions and the two oblique directions. The derivation of the maximum curvatures is based on the first and second derivatives in one of the four directions of the image. The implementation used in this research calculates the derivatives based on the scale space model. The derivatives are derived by convolving the image with the derivatives of a Gaussian function. An example image with its extracted

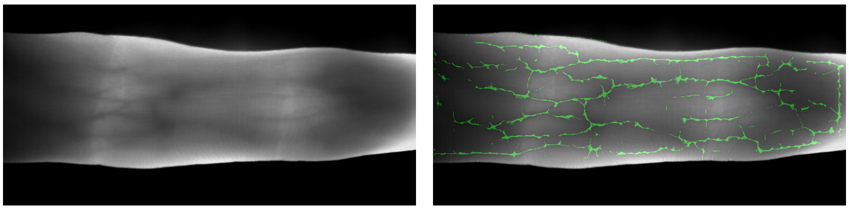

(a) Original image (b) Binarised vessels overlaid

Figure 5.4: Miura's maximum curvature method using sigma=5

features can be seen in Figure 5.4. The image on the left is the original image and the image of the right show the original image with the extracted vascular features imposed in green. The functionality of this method is provided by a custom Matlab function called `miura_max_curvature()`. The paper describing this method is not very clear about the method used for binarisation. It only states that the dispersion between the two groups in the locus space should be maximized. In this research the median of the locus space is used as a threshold. This binarisation method is also used in Miura's repeated line tracking method.

5.4.3 Miura's repeated line tracking method

This is another popular method for feature extraction and was proposed in 2004. This method [22] starts several times at random positions in the image and attempts to track a line. If pixels are tracked multiple times as being a line, these pixels have a high likelihood of being part of a blood vessel. The binarised result of the repeated line tracking method can be seen in Figure 5.5. For this

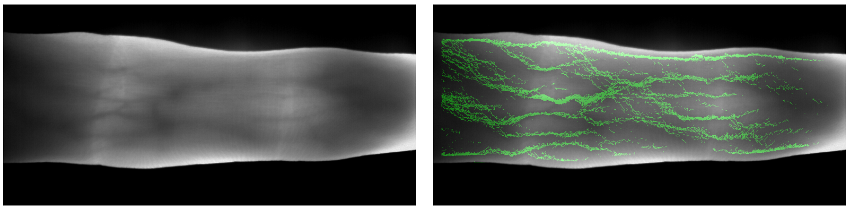

(a) Original image (b) Binarised vessels overlaid

Figure 5.5: Miura's repeated line tracking method using 1000 iterations, $r = 1$ and $W = 33$

image a thousand starting positions were used within the detected finger region. The functionality of this method is provided by a custom Matlab function called `miura_repeated_line_tracking()`. A downside of this Matlab implementation is that it is very slow because of the large number of iterations done. Because of this slow performance a crude C++ implementation has been made using the OpenCV libraries which is significantly faster.

5.4.4 Miura's matching method

This method for matching two sets of binarised feature images is described in the repeated line tracking paper by Miura et al. The method is also used in the maximum curvature method and by some others [8, 2]. This method is in fact just a correlation, the reference data is trimmed by a certain amount and is correlated with the input matching data. The maximum value of the correlation is normalized and used as matching score. The correlation is calculated as follows:

$$N_m(s,t) = \sum_{y=0}^{h-2c_h-1} \sum_{x=0}^{w-2c_w-1} I(s+x, t+y) R(c_w+x, c_h+y) \tag{5.2}$$

In this relation $N_m(s,t)$ is the correlation value between the trimmed reference image $R(x,y)$ and the input image $I(x,y)$. The width and height of both reference and input image is w by h pixels. The reference image is trimmed by c_h pixels at the top and bottom and by c_w pixels at the left and right of the image. The size of the correlation matrix is thus $2c_h$ by $2c_w$. The maximum value of this correlation, $N_{m_{max}}$ matrix is normalised and used as matching score. The normalisation is done as follows:

$$score = \frac{N_{m_{max}}}{\sum\limits_{y=t_0}^{t_0+h-2c_h-1} \sum\limits_{x=s_0}^{s_0+w-2c_w-1} I(x,y) + \sum\limits_{y=c_h}^{h-2c_h-1} \sum\limits_{x=c_w}^{w-2c_w-1} R(x,y)} \tag{5.3}$$

In this equation the indices s_0 and t_0 are the indices of the maximum value in the correlation matrix $N_m(s,t)$. Note that the score value will lie in the range $0 \leq score \leq 0.5$. This is a bit strange as the histogram in the original paper shows an x-axis which ranges from 0 to 0.7. Also note that in the original paper a so called mismatch ration is calculated, this is just one minus the score.

5.4.5 Choi's principal curvature method

The method described by Choi et al. [2] is based on the eigenvalues of the Hessian matrix. The blood vessels in the captured images can be regarded as line structures. Line structures show themselves in the image as local neighbourhoods in which the second derivative across the line is large, and the second derivative along the line is small. These second derivatives follow from the Hessian matrix. The second derivatives along and across the line are found as the eigenvalues of the Hessian matrix. The Hessian matrix has two eigenvalues, but only the first eigenvalue is used. The result before binarisation can be seen in Figure 5.6. The

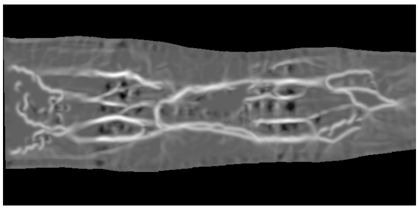

(a) Result before binarisation

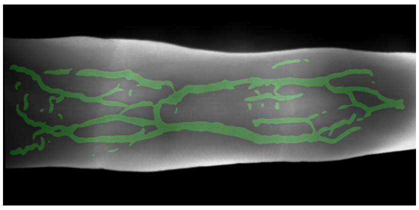

(b) Binarised vessels overlaid

Figure 5.6: Choi's principal curvature method using sigma=5 and a threshold of 1.6%

binarisation is done using Otsu's method which is the same as k-means with two clusters. The matching mentioned in the paper is done by translating and rotating the input image and determining the correlation. The translation is limited to ± 64 and ± 32 pixels for the horizontal and vertical directions. The rotation is limited to ± 10 degrees. The resolution for translation and rotation is 1 pixel and 1 degree respectively. This would mean that per correlation value $128 \times 64 \times 20 = 163840$ correlation coefficients need to be calculated. The computation time would be too large, therefore the matching method of Miura et al. was used in the verification of this algorithm. The rotation in the xy-plane has already been compensated for by the normalisation step.

5.4.6 Huang's wide line detector

The method described by Huang et al. [8] is similar to adaptive thresholding. Each pixel (x_0, y_0) in the image has a circular neighbourhood with radius r. For each of the pixels in this neighbourhood the difference with the central pixel (x_0, y_0) is determined. The number of pixels in this neighbourhood which have a difference smaller than a certain threshold are determined. This number is thresholded again to get a binary vascular image.

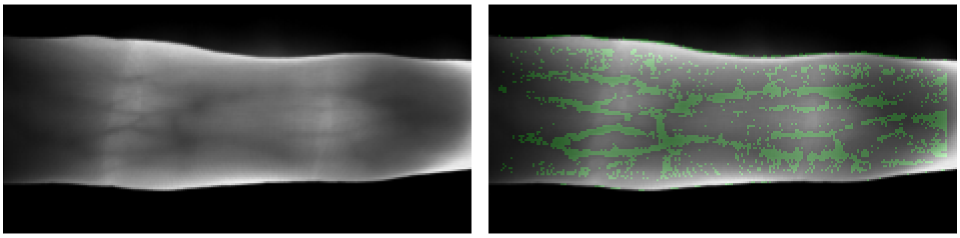

(a) Result before binarisation (b) Binarised vessels overlaid

Figure 5.7: Hunag's wide line method using $r = 5$,$t = 1$ and $g = 41$

Chapter 6

Results

This chapter will focus on the results obtained from the data collected during the pilot and the results from the verification experiments. The first section will elaborate on the method used to calculate the performance figures of an algorithm. The section after this will look at whether the vascular pattern is influenced by stressing or cooling the finger. This is done using the data collected during the pilot. At the end of this chapter the verification of several algorithms is performed using the dataset from the Peking university and the collected dataset.

6.1 Performance reporting

Before reporting any performance figures a consensus about how these figures are determined has to be made first. The experiments in this research are verification experiments, which are one-to-one comparisons. The goal of verification is to verify a claimed identity. There are two possible outcomes in a verification experiment, either the claimed identity is valid or not valid. The validation decision is governed by the system threshold t. There are two important rates in verification, the False Match Rate ($FMR(t)$) and the False Non-Match Rate ($FNMR(t)$), both these rates are a function of the system threshold t. The false match rate is the expected probability that an imposter is wrongly accepted and the false-non match rate is the expected probability that a true identity is wrongly rejected.

In this research two different methods for determining the $FMR(t)$ and $FNMR(t)$ curves are used. The first method divides the possible range of thresholds into uniform intervals called bins. For each bin the number of scores falling into it are determined. Both the performance results and the shape of the histogram depend on the number of bins used, hence when showing the histogram the number of bins used is mentioned. The other method uses the existing score levels as threshold. An advantage of this method is that no binning is necessary but a downside is the slow computation of this method as each score level is used as a threshold. For a quick evaluation the binning method is used, but when determining the actual performance the later method will be used. When the number of matches done is large and when the right number of bins is chosen both methods will approximate each other.

An important measure describing the performance of a biometric systems is the Equal Error Rate(EER). At this rate the number of false rejections and false acceptances are equal, i.e., the intersection point of the $FMR(t)$ and the $FNMR(t)$ curves. A simple but naive approach for determining this point is by determining the threshold t_{opt} which corresponds to the minimum value of $|FMR(t) - FNMR(t)|$. At this point the average between the two can be calculated and this can be used as the EER.

$$EER_{naive} = \frac{FMR(t_{opt}) + FNMR(t_{opt})}{2} \tag{6.1}$$

Due to the fact that the $FMR(t)$ and $FNRM(t)$ are not continuous curves the intersection cannot be directly determined with high precision, the 'real' intersection point is either right or left of the determined point. Figure 6.1 shows both possibilities, the first graph shows the situation where the determined EER point is right of the intersection and the second graph shows the reverse situation.

A better approach would be to fit a straight line through the surrounding points and determine the intersection of these two lines. The slope and offset of both fitted straight lines can be calculated. Using these parameters an intersection point can be determined. This method will be used during this research for determining the EER and the corresponding threshold. A more

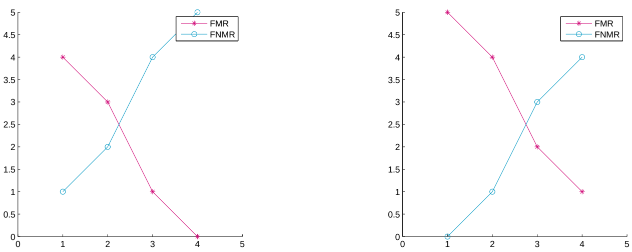

(a) Intersection right

(b) Intersection left

Figure 6.1: Two fictive $FMR(t)/FNRM(t)$ plots.

advanced method would be to fit a higher order line through these points to get a more accurate estimate of the EER. Giving confidence intervals for the EER is difficult as it depends on the intersection of two curves which both consist of a different number of measurements.

6.2 Results from pilot

To check whether temperature or stressing the fingers has an influence on the number of extracted features the normal condition fingers are compared with the cooled and stressed fingers. The method used for extracting the vascular features was Choi's principal curvature method. The captured images have been downscaled and trimmed a bit first. Part of the sensor was still visible on the left part of the image, hence a slice of 100 pixels wide has been trimmed of the images. The resulting image has been downscaled to 457×267 pixels to save

	normal	stressed	cold
normal	5.81	–	–
stressed	3.79	0.63	–
cold	4.92	1.52	3.03

Table 6.1: EER (%) for various matching options

computation time. The parameters for Choi's method are a sigma of four and a threshold of 1.3%. After binarisation the total number of vascular features are counted in each image. The reference number of vascular features is obtained by averaging the number of vascular features in the first two measurements. The percentual increase in vascular features is calculated by comparing the number of vascular features in the stressed and cold finger images to the reference number of features. Figure 6.2 shows the average percentual increase in the number of vascular features per finger. Fingers 1–3 belong to the left hand and fingers 4–6

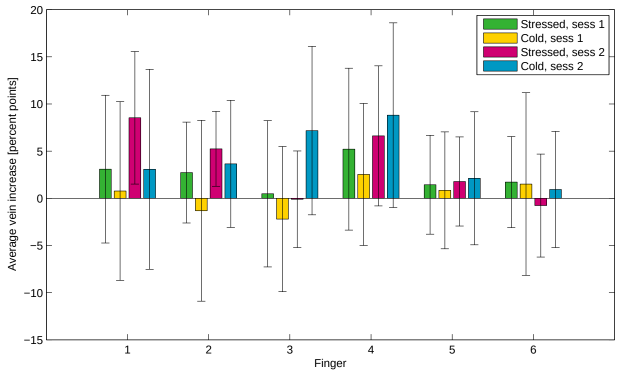

Figure 6.2: Influence of temperature and physical labour on the number of vein features.

belong to the right hand. The error-bars indicate the standard deviation of the measurements. None of the fingers show the expected behaviour, which is an increase for stressed fingers and a decrease for cooled fingers. Also the variation of the measurements is large.

The influence of stress and cold can also be investigated by determining the performance. The performance has been tested using Miura's maximum curvature method with a sigma of three. The finger region has been found using Lee's method and the finger has been normalised using Huang's method. For matching Miura's method has been used with a c_w of 25 and a c_h of 50. Various matching configurations have been tried and are summarised in Table 6.1. During these tests the images from both measurement sessions have been combined. It is remarkable to see that matching normal to normal conditions has the highest EER. For this normal condition images the difference between same day captured images and two week time difference images have been investigated. It was noticed that the same day EER was 5.30% and that the two week delay EER was 6.06%. Furthermore the difference between genders has been tested using only the normal condition images, these results were remarkable as the EER for females was 10.19% and that for the males this was 4.17%.

Finally it should be noted that no real conclusions can be drawn from these performance figures as the number of test persons was low. The gender differences and time differences will be investigated using the data from the real data collection.

6.3 Performance of the algorithms

The first three sections provide some background information on the testing methods used for determining the performance of various algorithms. Several authors have been contacted to ask for their implementation of the algorithms, but this gave no results. This is why the algorithms have been implemented by myself based on the information given in the papers. The correctness of these algorithms can not be verified as there are no reference implementations.

6.3.1 Testing method in general

Unless noted otherwise the images have not been downscaled. If a downscaling was performed it was done by using Matlab its `imresize()` function which is part of the Image Processing Toolbox. For all tests the `lee_region()` method has been used for detecting the region of the finger. Unless mentioned otherwise the size of the mask was 40×4 for this method. All fingers have been normalised using Huang's method.

Each of the algorithms is tested with images which have not been subjected to any pre-processing steps and images which are pre-processed using adaptive histogram equalisation. This adaptive histogram equalisation was described earlier in Section 5.3.

To save computation time when determining the performance only half of the possible tests are done, this can be done because matching A with B is roughly the same as matching B with A.

For each of the algorithms the Detection Error Trade-off (DET) curves are given for both datasets, with and without adaptive histogram equalisation. The term *AHE* has been used in the figure legends to refer to the usage of adaptive histogram equalisation. Also the performance in terms of EER will be given.

6.3.2 Testing method for the Peking dataset

The Peking University Finger Vein database (V4) consists of 200 directories containing varying amounts of finger vascular pattern images. The width of blood vessels in these images range from 5–15 pixels. In this research only directories containing exactly eight finger vascular images are used for testing. This accounts for 153 usable directories available for testing. Ten percent of these directories (15) are used for determining the optimal parameters for the lowest possible EER. The number of genuine tests which can be done with these 15 directories is 420 and the number of imposter tests which can be done is 6720. When the optimal parameters have been found the other 90%, which corresponds with 138 directories, are used for actual testing. The number of genuine attempts which can be done in this case is 3864 and the number of imposter tests which can be done is 604992.

The images in this database contain an eight by eight pixel number three in the upper-right and lower-right corner. This number can be clearly seen in Figure 6.3. This number has an abrupt change in intensity compared to the background which will interfere with the detection of the finger region. In order to get a correct estimate of the finger region the top-right and lower-left corner numbers are replaced by the average intensity of the surrounding pixels. This ensures a correct detection of the finger region. The functionality of this simple fix is provided by the custom Matlab function `pku_fix()`.

6.3.3 Testing method for the Twente dataset

The Twente dataset consists of 354 unique fingers collected from 59 volunteers. Each finger has been captured four times in total. For this dataset also 10% has been used for training. This means 35 fingers have been used for training and that 319 finger are used for the real testing. The 35 training fingers are all from different fingers from different volunteers. For training the number of genuine tests which can be done is 210 en the number of imposter tests which can be done is 9520.

For the real test with 319 fingers the number of genuine tests which can be done is 1914 and the number of imposter tests which can be done is 811536.

There are still a few doubts about using 10% of the fingers instead of 10% of the volunteers for training. When using 10% of the fingers this already covers more then half of the volunteers. Earlier it was noted that the variance in quality of the images from the same person is low. On the other hand when using 10% of the people for training it is not possible to get satisfactory training results as the algorithms perform too well in some cases.

6.3.4 Normalisation

The finger with the largest detected area of the Peking dataset is the second image of the 18440 directory. This image can be seen on the left of Figure 6.3. The detected finger region for this finger is correct. The image with the largest rotation is the first image of the 1650 directory. This image can be seen on the right of Figure 6.3. The estimated rotation of this finger was 8.6 degrees. This image also has the largest estimated translation and the smallest detected finger region area. This due to the fact that the finger region is not correctly detected. As mentioned before the region detection algorithm assumes that the lower half of the finger is in the lower half of the image. Which is not the case for this particular image.

From the Twente dataset the finger with the largest detected area was finger number three from volunteer number 10. The finger with the smallest detected area was finger number one from volunteer number 21. The largest detected rotation was 6.6 degrees, this was finger number five from volunteer number 40. The corresponding images can be seen in Figure 6.4. The finger with the largest detected area could not be displayed as the volunteer did not give permission for this.

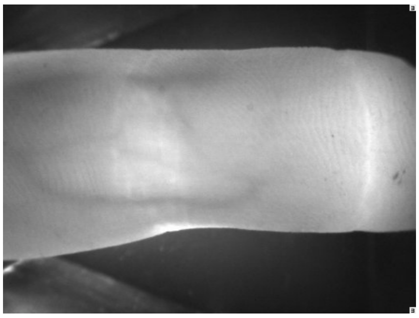

(a) Finger with the largest area

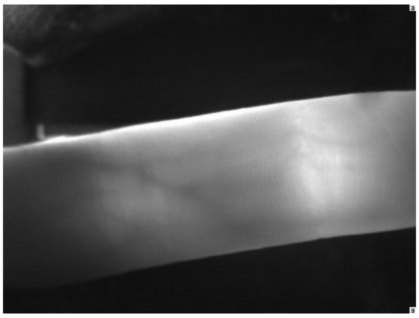

(b) Finger with the largest rotation

Figure 6.3: Finger with the largest rotation and area

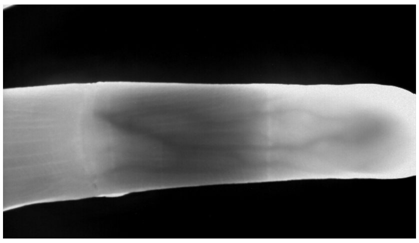

(a) Finger with the smallest area

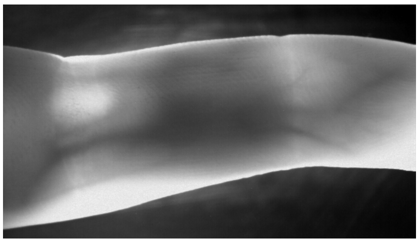

(b) Finger with the largest rotation

Figure 6.4: Finger with the largest rotation and the smallest area

6.3.5 Normalised cross-correlation

To get some kind of reference for comparing the other algorithms with the normalised cross-correlation is chosen as it is one of the most basic methods. Before performing the cross-correlation the finger regions are detected and the fingers are normalised. In order to calculate a cross-correlation the template must be equal or smaller than the reference image. Based on the training set the optimal size of the template for the Peking dataset was obtained by trimming 24 pixels from the top and bottom and trimming 12 pixels from the left and right of the image. For the Twente dataset 5 pixels were trimmed from the top and bottom and no pixels were trimmed from the left or right of the image. For the Peking dataset the EER was 14.67% when not using adaptive histogram equalisation and with this pre-processing step the EER was 9.81%. The respective performance figures for the Twente dataset were 3.15% and 1.99 %. The corresponding DET curves can be seen in Figure 6.5.

6.3.6 Miura's maximum curvature

The sigma used for this method was five for both the Peking dataset and the Twente dataset. For the Peking dataset the parameters for Miura's matching method were $c_w = 98$ and $c_h = 86$.

For the Twente dataset it was difficult to estimate good c_w and c_h values as the EER was zero for several of the possible c_w and c_h values. Eventually

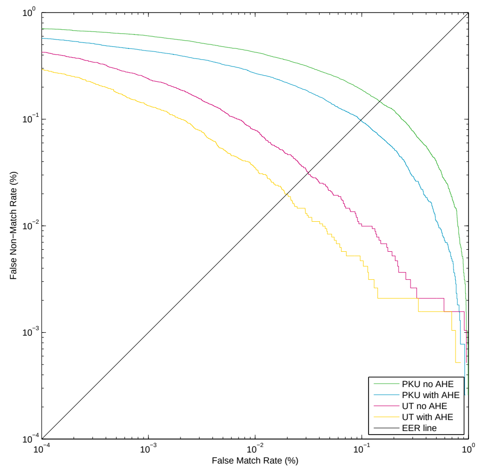

Figure 6.5: DET curve for normalised cross-correlation

the parameters for Miura's matching method for the Twente dataset were set to $c_w = 90$ and $c_h = 80$. For the Peking dataset the EER was 1.22% when not using adaptive histogram equalisation and with this pre-processing step the EER was 1.32%. The respective performance figures for the Twente dataset were 0.63% and 0.49 %. The corresponding DET curves can be seen in Figure 6.6.

6.3.7 Miura's repeated line tracking

The parameters used for the Peking dataset are 2000 iterations with $r = 1$ and $W = 23$. The matching is done by Miura's method again with $c_w = 98$ and $c_h = 86$.

To decrease the computation time when using the Twente dataset the images have been downscaled by a factor of 0.6 and the resulting images are 404×228 pixels. Using the training set the optimal parameters have been determined to be 3000 iterations, $r = 1$ and $W = 21$. The parameters for matching were set to $c_w = 55$ and $c_h = 65$. For the Peking dataset the EER was 6.75% when not using adaptive histogram equalisation and with this pre-processing step the EER was 5.90%. The respective performance figures for the Twente dataset were 1.04% and 0.99 %. The corresponding DET curves can be seen in Figure 6.7. The big difference in performance of the Peking and the Twente dataset might suggest that the parameters used for the Peking dataset are not optimal.

6.3.8 Choi's principal curvature

For the Peking dataset the images have been downscaled by a factor of 0.6 and the resulting images are 308×231 pixels. The images of the Twente dataset have not been downscaled. The parameters used for feature extraction are the same for both datasets and compromise a sigma of 2 and a threshold of 1.3%. The binarisation of the resulting images is done using Otsu's method. For the

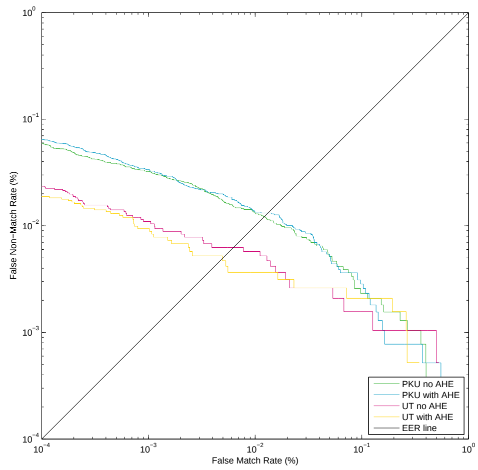

Figure 6.6: DET curve for Miura's maximum curvature

Peking dataset the Miura matching method the parameters c_w and c_h are set to 64 and 79 respectively. For the Twente dataset these parameters were set to 38 and 22. For the Peking dataset the EER was 2.72% when not using adaptive histogram equalisation and with this pre-processing step the EER was 2.20%. The respective performance figures for the Twente dataset were 0.89% and 0.37 %. The corresponding DET curves can be seen in Figure 6.8.

6.3.9 Huang's wide line detector

The images of the datasets have been downscaled to approximate the finger width of the images used in the original paper. For the Peking dataset this meant that the images had to be downscaled by a factor of 0.35. The resulting images have a size of 180×135 pixels. The images of the Twente dataset have been downscaled by a factor of 0.24 for the same reason and the resulting images have a size of 162×92 pixels. Because the images have been downscaled the mask used in Lee's region detection method had a width of 10 and a height of 4.

The parameters for the wide line detector are the same as used in the original paper $r = 5, t = 1, g = 41$. The matching method used is Miura's method. For the Peking dataset $c_w = 22$ and $c_h = 4$ for the Twente dataset this was $c_w = 28$ and $c_h = 18$. For the Peking dataset the EER was 4.66% when not using adaptive histogram equalisation and with this pre-processing step the EER was 2.73%. The respective performance figures for the Twente dataset were 1.72% and 0.89 %. The corresponding DET curves can be seen in Figure 6.9.

6.3.10 Summarising

A table which summarises all of the mentioned performance figures is given in Table 6.2. The table shows the performance of both datasets with and without adaptive histogram equalisation. It also shows the performance which has been

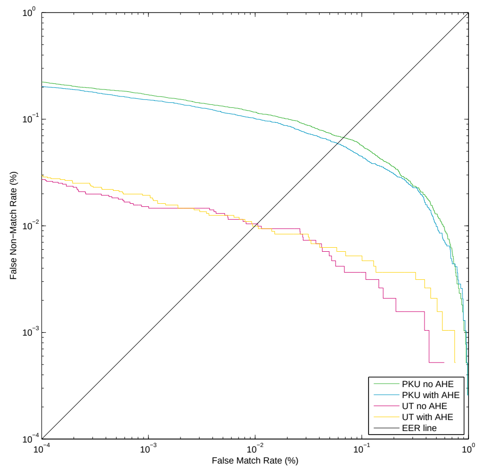

Figure 6.7: DET curve for Miura's repeated line tracking

		Peking		Twente	
	original paper	no AHE	with AHE	no AHE	with AHE
Normalised cross-correlation	0.00	14.67	9.81	3.15	1.99
Maximum curvature	0.00	1.22	1.32	0.63	0.49
Repeated line tracking	0.15	6.75	5.90	1.04	0.99
Principal curvature	0.36	2.72	2.20	0.89	0.37
Wide line detector	0.87	4.66	2.73	1.72	0.89

Table 6.2: Performance of several algorithms for both datasets, both with and without adaptive histogram equalisation (AHE).

achieved in the actual paper in the second column. All of these papers made use of their own collected dataset.

As it can be seen the application of adaptive histogram equalisation enhances the performance of nearly all the algorithms. The only exception is the maximum curvature method using the Peking dataset. The table also shows that the performance of the Twente dataset is higher in all cases. Using the Twente dataset the performance of the principal curvature method and the wide line detector method have approximated the value mentioned in the literature.

6.3.11 Miscellaneous experiments

As the collected dataset contains meta-information about gender and handedness several interesting experiments can be done. These are described in the consecutive subsections. The scores from Miura's maximum curvature method with adaptive histogram equalisation have been used for these experiments.

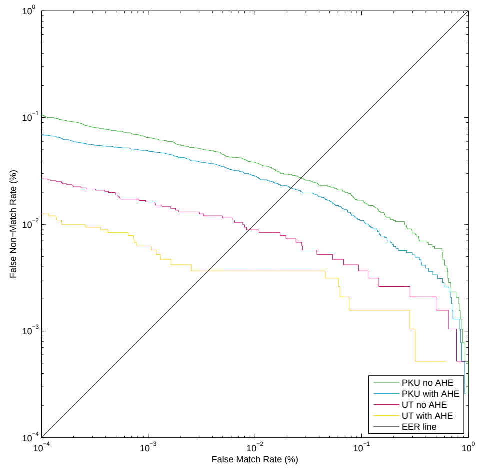

Figure 6.8: DET curve for Choi's principal curvature

Time interval

The dataset contains images of the same finger with very small time between capturing moments and images with a large amount of time between capturing moments. The time difference for the small time interval images was about ≈2–3 minutes. The large time difference was approximately two weeks. When comparing small time difference images with each other the performance is 0.314% and when comparing images with large time difference the performance is 0.531%. The number of genuine tests for the small time difference images was 638 and the number of imposter tests was 405768. For the large time difference images these figures were 1276 genuine tests and 405768 imposter tests. From this experiment it can be concluded that for determining realistic performance figures it is essential to have data with a large time difference between capturing moments.

Gender

The dataset also enables the investigation of gender differences on the performance. The dataset consists of 44 males and 15 females. When considering only males in the dataset the performance is 0.278% and when considering only females in the dataset the performance is 1.177%. The number of genuine tests done for males was 1440 and for females the number of tests was 474. The number of imposter tests done for males was 458880 and for females this was 49296. The lower performance for females might be caused by the fact that females have lower haemoglobin levels compared to men. The reliability of these findings is not very high as the number of volunteers is low.

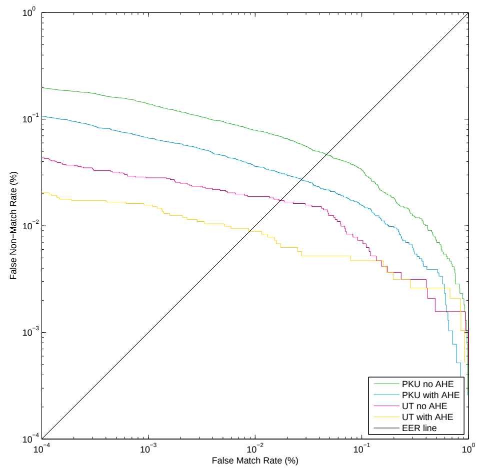

Figure 6.9: DET curve for Huang's wide line detector

finger	1	2	3	4	5	6
performance (%)	0.315	0.327	0.943	1.258	0.018	0.066

Table 6.3: Performance in terms of EER for different fingers.

Finger

For the performance evaluation it was assumed that all six finger were identical individualities of the same class and could be interchanged with one another. For instance matching the ring finger of the left hand with the middle finger of the right hand was considered as a valid imposter attempt. During the collection of the Twente dataset it was noticed that index and ring fingers tend to curve towards the middle finger. This observation might mean that fingers have to be treated as different classes. The work by Kumar et al. [14] already observed that the performance of middle fingers was worse when compared to index fingers. They attribute this to the difference in convenience when capturing the fingers.

In this research the difference between fingers is also investigated in terms of performance. Therefore the dataset is divided into six classes, one for each finger. The number of genuine test for fingers 1–5 was 318 and for finger 6 this was 324. The number of imposter tests for fingers 1–5 were 22048 and for finger 6 this was 22896. The performance results per finger are given in Table 6.3. For the left hand the observation does not match with the findings by Kumar et al.. Note that Kumar et al. only collected data from the left hand of the volunteers so it can not be verified whether the findings are in correspondence with the right hand of the volunteers. It is interesting to see that the index fingers have the worst performance compared to the other fingers. For the right hand it is remarkable to see that the middle finger performs significantly better than the surrounding fingers.

Chapter 7

Conclusion and recommendations

This research has focused on three things mainly, the first focus point was the design of a sensor which is capable of capturing images of the vascular pattern of the finger. The second focus point was the collection of a dataset of vascular pattern images of the finger for release to the research community and to verify the performance of existing algorithms. The last focus point was the verification of several algorithms mentioned in the literature using the collected dataset and an existing dataset.

The collected dataset is a noteworthy contribution to the field of finger vascular pattern biometrics. The collected dataset consist of 59 volunteers which had their ring, middle and index finger from both hands captured. Each finger has been captured four times, twice during the first session and twice during the second sessions which was two weeks later. One of the key features of this dataset is the high quality of the images and the availability of meta information about the volunteers. The meta information collected is the finger type, age, gender and handedness of the volunteers. Furthermore the resolution of the captured images is known which makes comparing performances with other future datasets easier.

The performance of the collected dataset and an existing dataset from the Peking University has been evaluated in terms of Equal Error Rate (EER). The achieved EER of of the existing dataset ranged from 14.67% up to 1.22%. For the collected dataset of this research the EER ranges from 3.15% up to 0.37%. The performance of the collected dataset was higher for all algorithms. Furthermore the effect of adaptive histogram equalisation on the performance has been evaluated. This has revealed that by using this pre-processing method the performance can be significantly improved.

As the collected dataset contains meta information about the volunteers the influence of several factors on the performance could be analysed. One of the most significant findings is that the quality of the images is probably gender dependant. When selecting only males from the dataset the performance is better compared to selecting only females from the dataset. Also the time between capturing moments influences the performance. For getting more realistic results there should be several weeks between enrolment and verification.

Returning to the question posed at the beginning of this study, it is now possible to state that this form of biometrics certainly has the potential of becoming the biometric of the future. But before this is the case more research is needed and larger datasets have to be collected which have a higher a resemblance to a real population.

7.1 Further work

This research has thrown up many questions in need of further investigation. For real applications a more 'open' sensor is preferred for a higher user convenience. For future work it is recommended to look at the design of an other sensor type such as a side illumination model. The side lighting method which places the illumination sources at an angle looks promising for this purpose. Another requirement necessary for real applications is some kind of liveliness detection to make sure the object presented is really a live human finger. Furthermore the optical properties of the mirror and the near infra-red filter used should be checked more thoroughly.

The current transillumination method for getting a uniform intensity across the entire image is rather slow and it might not produce the optimal results. Future research should focus on better algorithms and increase the speed of adjustment. This speed enhancement can be achieved by using a more low level programming level instead of Matlab.

In the future it might even be possible to detect diseases with this type of sensor. For example, patients with rheumatism might be detectable by the way the light is transmitted through their interphalangeal joints.

The roll around the x-axis of the finger when capturing images might be solved by generating a three dimensional model of the vascular pattern by using multiple mirrors. Another point which needs attention is the translation of the finger in the x-direction. As mentioned earlier this might be solved by detecting the position of the interphalangeal joint.

In this research only high level features have been investigated. It would also be interesting to investigate more low level feature extraction methods such as principal component analysis (PCA) or linear binary patterns (LBP). To increase the performance the score of the vascular pattern biometric can be combined with other features such as the shape of the finger which is already present in the captured image. By using a 'hot-mirror' it is possible to capture a vascular pattern image and a crease patten image at the same time. The scores of these two types of images can be fused to get a higher performance [14].

Appendix A

Volunteer consent form

The volunteer consent form has been added as a reference in the following two pages.

Information letter for participants of a study on finger vein biometrics.

Purpose of the study

Finger vein recognition is advertised as a promising biometric, characterized by very low error rates, good spoofing resistance, and a user convenience that is equivalent to that of fingerprint recognition. At present manufacturers keep most of their technology secret. As a result of this there are only a few publically available datasets and only little academic research has been done in order to verify published claims on performance. The purpose of this research is to acquire a database of finger vein images for verification and testing.

What is your contribution to this research?

A number of images of the vascular pattern of your fingers will be captured at several occasions. These images, along with your age, gender, handedness and a sequential number will be stored in a database. This data will be used for research. Your contribution is valuable for the creation of a database containing images of the vascular pattern of the finger.

Confidential

All participants are given a unique identification number and your data will be processed anonymously. All legal rules for data storage will be applied.

Risks

The setup for acquiring images of the finger vascular pattern makes use of high power near-infrared Light Emitting Diodes (LEDs). As far as we know, no long or short term effects of this near-infrared light on the skin or to the eye are known. Nonetheless, participation in this research is at your own risk.

Who will carry out the research?

The research will be conducted by B. Ton BSc (b.t.ton@alumnus.utwente.nl) on behalf of Dr. Ir. R.N.J. Veldhuis (r.n.j.veldhuis@utwente.nl). If you have any further questions about the research, you can contact Mr. Ton or Mr. Veldhuis via email. If in any case or at any time, you wish to withdraw your data from the research program you can contact one of the above mentioned persons.

We thank you in advance for your participation in this research.

Sincerely,

Bram Ton
Master student Electrical Engineering

Volunteer consent form

The study in which we ask you to participate entails that we record a number of images of the vascular pattern of your fingers at several occasions. Furthermore your gender, age and handedness will be recorded.

That is all we ask from you. No further investigation is necessary and you do not have to provide any further information to us. Of course, your data is processed anonymously and confidentially.

If you are willing to participate in this research, then please read the statement below and sign this declaration.

I confirm that I read the information letter and have been properly informed about the nature of the investigation, which is the collection of a database containing vascular patterns of the finger.

I willingly participate in these trials at my own risk. I consent to images of the vascular pattern of my fingers and my questionnaire responses being collected during the trial and stored electronically. I agree to the use of this data by the University of Twente and any other research for the purposes of evaluating the performance of biometric systems and identifying problems and improvements.

I understand that my name/identity will not be stored or shown in any released database or report. Furthermore I understand that images from the database might be included in published work, unless an objection is given.

Date :

Name :

Signature :

Optional:

- ☐ I object to the inclusion of my captured vascular pattern images in any publications.

Appendix B

Sensor details

B.1 Dimensions of the sensor

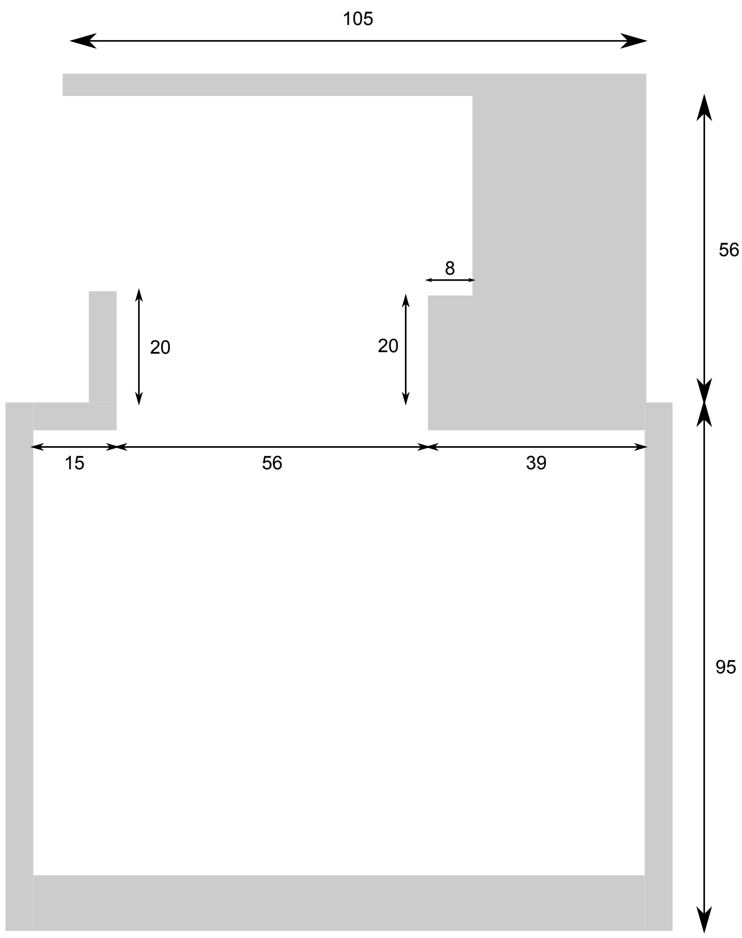

Figure B.1: Cross section of the sensor

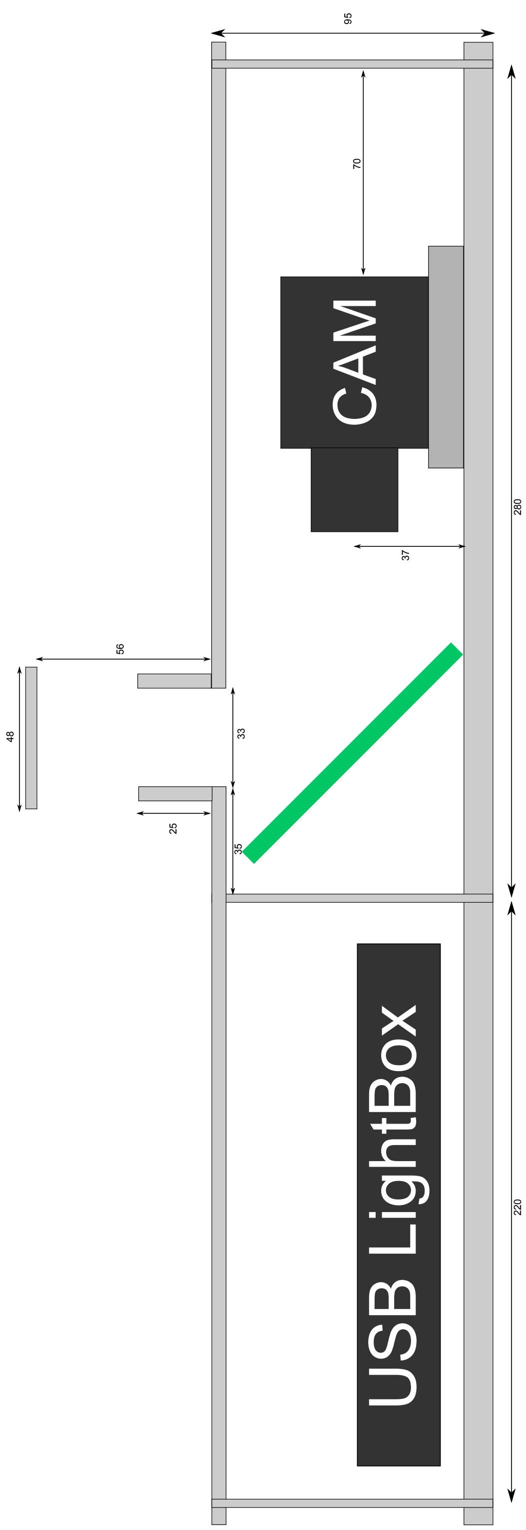

Figure B.2: Cross section of the sensor

B.2 Transillumination method

This simple LED adjustment control loop has been used for collecting the data for the pilot and the real dataset. The flow chart of this control loop can be seen in Figure B.3. The maximum PWM value was set to 0.8 and the PWM step

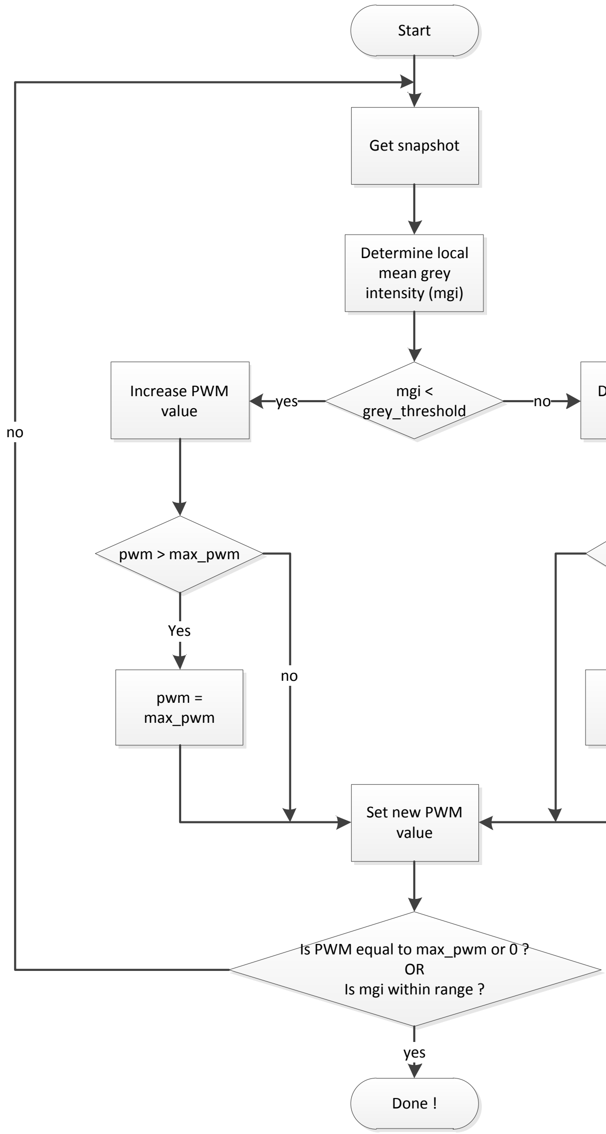

Figure B.3: Flowchart for the LED power adjustment control loop

size was set to 0.04. The local mean grey intensities were determined directly underneath the LEDs using a square window of 40 by 40 pixels. The grey level threshold was set to 80 and the maximum deviation allowed from this threshold was 20%. The current implementation starts with a PWM value of zero which is not very time efficient. In the future it might be beneficial to start with an average initial value to decrease the regulating time.

Bibliography

[1] B. Bradtmiller et al. *Anthropometric Survey of Federal Aviation Administration Technical Operations Personnel*. 2008.

[2] J.H. Choi et al. "Finger vein extraction using gradient normalization and principal curvature". In: ed. by Kurt S. Niel and David Fofi. Vol. 7251. 1. San Jose, CA, USA: SPIE, 2009, p. 725111. DOI: 10.1117/12.810458.

[3] Y. Dai et al. "A Method for Capturing the Finger-Vein Image Using Nonuniform Intensity Infrared Light". In: *Congress on Image and Signal Processing* 4 (May 2008), pp. 501–505. DOI: 10.1109/CISP.2008.654.

[4] European Parliament, Council. "Directive 2006/25/EC of the European Parliament and of the Council of 5 April 2006 on the minimum health and safety requirements regarding the exposure of workers to risks arising from physical agents (artificial optical radiation) (19th individual Directive within the meaning of Article 16(1) of Directive 89/391/EEC)". In: *Official Journal of the European Union*. L 114. Apr. 2006, pp. 38–59. URL: http://eur-lex.europa.eu/LexUriServ/LexUriServ.do?uri=CELEX:32006L0025:EN:NOT.

[5] "Finger Vein Authentication Unit". US 2011/0222740 A1. 2011.

[6] Hitachi, Ltd. *Finger Vein Authentication: White Paper*. 2006.

[7] Hitachi, Ltd. *Hitachi develops a 3mm thin-type finger vein authentication module*. Aug. 2009. URL: http://www.hitachi.com/New/cnews/090826.html.

[8] B. Huang et al. "Finger-Vein Authentication Based on Wide Line Detector and Pattern Normalization". In: *20th International Conference on Pattern Recognition*. Aug. 2010, pp. 1269 –1272. DOI: 10.1109/ICPR.2010.316.

[9] International Biometric Group. *Comparative Biometric Testing - Round 6 Public Report*. Sept. 2006.

[10] H. W. Jürgens, I. Matzdorff, and J. Windberg. "International Anthropometric Data. International Anthropometric Data for Work-Place and Machinary Design". In: *Arbeitswissenschaftliche Erkenntnisse: Forschungsergebnisse für die Praxis*. 108e. Bundesanstalt für Arbeitsschutz und Arbeitsmedizin, 1998.

[11] B.J. Kang and K.R. Park. "Multimodal biometric method based on vein and geometry of a single finger". In: *IET Computer Vision* 4.3 (Sept. 2010), pp. 209–217. ISSN: 1751-9632. DOI: 10.1049/iet-cvi.2009.0081.

[12] J. Kim et al. “Non-contact finger vein acquisition system using NIR laser”. In: *Sensors, Cameras, and Systems for Industrial/Scientific Applications X*. Vol. 7249. Proceedings of SPIE-IS&T Electronic Imaging. SPIE, Jan. 2009. DOI: 10.1117/12.810563.

[13] M. Kono, H. Ueki, and S. Umemura. “Near-Infrared Finger Vein Patterns for Personal Identification”. In: *Appl. Opt.* 41.35 (Dec. 2002), pp. 7429–7436. DOI: 10.1364/AO.41.007429.

[14] A. Kumar and Y. Zhou. “Human Identification Using Finger Images”. In: *IEEE Transactions on Image Processing* 21.4 (Apr. 2012), pp. 2228 –2244. ISSN: 1057-7149. DOI: 10.1109/TIP.2011.2171697.

[15] E.C. Lee, H. Jung, and D. Kim. “New Finger Biometric Method Using Near Infrared Imaging”. In: *Sensors* 11.3 (2011), pp. 2319–2333. DOI: 10.3390/s110302319.

[16] E.C. Lee, H.C. Lee, and K.R. Park. “Finger vein recognition using minutia-based alignment and local binary pattern-based feature extraction”. In: *International Journal of Imaging Systems and Technology* 19.3 (Sept. 2009), pp. 179–186. DOI: 10.1002/ima.20193.

[17] E.C. Lee and K.R. Park. “Image restoration of skin scattering and optical blurring for finger vein recognition”. In: *Optics and Lasers in Engineering* 49.7 (Mar. 2011), pp. 816–828. DOI: 10.1016/j.optlaseng.2011.03.004.

[18] E.C. Lee and K.R. Park. “Restoration method of skin scattering blurred vein image for finger vein recognition”. In: *Electronics Letters* 45.21 (Aug. 2009), pp. 1074–1076. ISSN: 0013-5194. DOI: 10.1049/el.2009.1231.

[19] S. Z. Li and A. Jain. *Encyclopedia of Biometrics*. Springer Science+Business Media, LLC, 2009. DOI: 10.1007/978-0-387-73003-5.

[20] A.J. Mansfield and J.L. Wayman. *Best Practices in Testing and Reporting Performance of Biometric Devices, Version 2.01*. Tech. rep. National Physical Laboratory, Aug. 2002.

[21] N. Miura, A. Nagasaka, and T. Miyatake. “Extraction of finger-vein patterns using maximum curvature points in image profiles”. In: *IAPR conference on machine vision applications*. 9. May 2005, pp. 347–350. URL: http://b2.cvl.iis.u-tokyo.ac.jp/mva/proceedings/CommemorativeDVD/2005/papers/2005347.pdf.

[22] N. Miura, A. Nagasaka, and T. Miyatake. “Feature extraction of finger vein patterns based on iterative line tracking and its application to personal identification”. In: *Syst. Comput. Japan* 35 (7 June 2004), pp. 61–71. DOI: 10.1002/scj.v35:7.

[23] J.F.M. Molenbroek and J.M.198 Dirken. *DINED 1982 Dutch adults*. 1982. URL: http://dined.io.tudelft.nl/ergonomics/.

[24] F. Mulvey et al. *D5.4 Exploration of safety issues in Eyetracking*. Communication by Gaze Interaction (COGAIN). 2008. URL: http://www.cogain.org/results/reports/COGAIN-D5.4.pd.

[25] D. Mulyono and H.S. Jinn. “A study of finger vein biometric for personal identification”. In: *International Symposium on Biometrics and Security Technologies*. Apr. 2008, pp. 1–8. DOI: 10.1109/ISBAST.2008.4547655.

[26] J. M. Murkin and M. Arango. "Near-infrared spectroscopy as an index of brain and tissue oxygenation". In: *British Journal of Anaesthesia* 103.Supplement 1 (2009), pp. i3–i13. DOI: 10.1093/bja/aep299.

[27] W. Pi, J. Shin, and D. Park. "An effective quality improvement approach for low quality finger vein image". In: *International Conference on Electronics and Information Engineering*. Vol. 1. Aug. 2010, pp. 424–427. DOI: 10.1109/ICEIE.2010.5559667.

[28] D. Wang, J. Li, and J. Memik. "User identification based on finger-vein patterns for consumer electronics devices". In: *IEEE Transactions on Consumer Electronics* 56.2 (May 2010), pp. 799–804. ISSN: 0098-3063. DOI: 10.1109/TCE.2010.5506004.

[29] G. Webster. *Biometric ATM gives cash via 'finger vein' scan*. July 2010. URL: http://articles.cnn.com/2010-07-05/world/first.biometric.atm.europe_1_banking-markets-polish-bank-bank-cards?_s=PM:WORLD.

[30] T. Yanagawa, S. Aoki, and T. Ohyama. "Human finger vein images are diverse and its patterns are useful for personal identification". In: *MHF Preprint Series* (2007). DOI: 10.1.1.97.4421.

[31] J. Yang, Y. Shi, and R. Wu. "Finger-Vein Recognition Based on Gabor Features". In: ed. by Z. Riaz. InTech, Oct. 2011. Chap. 2, pp. 17–32. URL: http://www.intechopen.com/books/show/title/biometric-systems-design-and-applications.

[32] Y. Yin, L. Liu, and X. Sun. "SDUMLA-HMT: A Multimodal Biometric Database". In: *Biometric Recognition*. Ed. by Zhenan Sun et al. Vol. 7098. Lecture Notes in Computer Science. Springer Berlin / Heidelberg, 2011, pp. 260–268. ISBN: 978-3-642-25448-2. DOI: 10.1007/978-3-642-25449-9_33.

[33] X. Yu et al. "A Novel Finger Vein Pattern Extraction Approach for Near-Infrared Image". In: *2nd International Congress on Image and Signal Processing*. Oct. 2009, pp. 1–5. DOI: 10.1109/CISP.2009.5304440.

[34] Z. Zhang, S. Ma, and X. Han. "Multiscale Feature Extraction of Finger-Vein Patterns Based on Curvelets and Local Interconnection Structure Neural Network". In: *The 18th International Conference on Pattern Recognition*. Vol. 4. Aug. 2006, pp. 145–148. DOI: 10.1109/ICPR.2006.848.